Water Budgets and Droughts under Current and Future Conditions in the Congo River Basin

Venkataramana Sridhar[1]*, Hyunwoo Kang[1], Syed A. Ali[1], Gode B. Bola[2], Raphael M. Tshimanga[2] and Venkataraman Lakshmi[3]

[1]Department of Biological Systems Engineering, Virginia Polytechnic Institute and State University, Blacksburg, VA 24061; vsri@vt.edu (corresponding author)

[2] Congo Basin Water Resources Research Center (CRREBaC), University of Kinshasa, Kinshasa, Democratic Republic of Congo

[3] Engineering Systems and Environment, University of Virginia Charlottesville VA 22904

Abstract

A multi-model hydrological assessment in the Congo Basin is performed to assess water availability conditions for historical and future periods (1913–2099). With models limited by scarce in situ observations, a combination of GRACE satellite data and soil-moisture-based drought indices is shown to be capable of estimating water budget, streamflow, and drought and storage variability. Changes in land use and land cover played a role in modifying the hydrologic responses but were found to be within the uncertainties of other inputs, including weather, soil, and model parameters. Seasonal and annual variability in total water storage anomalies (TWSAs) and the modified Palmer drought severity index (MPDSI) display a good correlation with each other. A selected set of global climate models is used to characterize the future temperature and precipitation patterns. It is expected that subbasin-scale variability in future temperature and precipitation increases will result in increased evapotranspiration, decreased runoff, and more drought events in the Congo Basin.

Key Words: Hydrology, Drought, Climate Change, Congo Basin

1. Introduction

Many studies have been carried out to quantify the interaction between climate, hydrology, and human-driven land-use change. Generally, these studies can be classified into two groups. The first group deals with natural, unmanaged rivers, where the drivers of change arise from climate and natural land transformation (Sridhar et al., 2013). The second group comes under the category of managed river basins, where water resources are heavily impacted by human-induced changes such as climate, land cover, agriculture, and population growth (Hoekema & Sridhar, 2013; Jaksa & Sridhar, 2015; Seong & Sridhar, 2017; Sridhar & Anderson, 2017). The Congo, the second-largest river basin in the world, provides 30% of Africa's freshwater resources (Alsdorf et al., 2016). The basin is underdeveloped and has not been studied extensively. Most studies focus on other large river basins, such as the Amazon, Mekong, and Mississippi, which has led to a limited understanding of the hydrology and drought conditions in the Congo Basin. This river is home to significant natural resources, but there were mismanagement, limited observational data, and political issues that have restricted the sustainable management of the Congo Basin (Runge, 2007). Although the river is used for hydropower generation and transportation, it remains relatively little polluted due to minimal agricultural activities. Jiang et al. (2019) reported that most parts of the Congo Basin are found to have a longer dry season during the boreal summer (June to August) and that the length of the dry season has increased between 6.4 and 10.4 days per decade in the period of 1988 to 2013. Thus, further investigation is required to investigate the changing water availability and drought conditions under climate change conditions. Accordingly, water storage assessment done elsewhere in the Chesapeake Bay and the Mekong showed that a combination of hydrological modeling and remote sensing data can be applied effectively to assess basin water resources (Ali & Sridhar, 2019; Sridhar et al., 2019).

48 It is also imperative to use simulated soil moisture for understanding the drought characteristics of
49 regions where in situ observations are limited. Climate change impacts in the form of droughts are
50 widely reported for several regions around the world, including India, the United States, and Southeast
51 Asia (Bisht et al., 2018; Kang & Sridhar, 2018a; Sehgal & Sridhar, 2018). Thilakarathne and Sridhar (2017)
52 mapped copula-based drought severity and frequency in the Mekong River Basin. Hydrological model
53 outputs, such as soil moisture, runoff, and evapotranspiration, have proven to be effective in
54 formulating drought indices (Kang & Sridhar, 2017, 2018b). In order to manage a river basin in the
55 context of the food-energy-water nexus and natural resources, an integrated assessment of the basin is
56 required. This includes assessing the shifts in hydrological regimes driven by climate variability and
57 changes in land cover and land use. Spatial variability in precipitation coupled with distinct seasonal
58 variability requires basin management and the assessment of remote sensing-based water storage
59 variability driven by these environmental changes. We hypothesize that a reduction in dry season flows
60 in a changing climate can worsen the drought conditions in the basin. The objectives of this research are
61 (1) evaluate the impacts of land use changes on hydrologic conditions using two land cover data (1992
62 and 2012), (2) assess the total water storage conditions integrated with hydrological models and remote
63 sensing, and (3) evaluate the availability of basin water resources using a model-driven drought index
64 simulated by hydrological models under various changing climate conditions.

65 **2. Background**

66 ***2.1. The Congo Basin***

67 The Congo Basin covers about 3.7 million km^2 and flows through several countries, including the
68 Democratic Republic of the Congo (DRC), the Republic of the Congo, portions of Cameroon, the Central
69 African Republic, Tanzania , Zambia, and Angola (Figure 1). Burundi and Rwanda are also linked to the

7

8

Congo Basin through lakes Tanganyika and Kivu, respectively. The basin is home to more than 100 million people and is largely underdeveloped; however, recent political stability has allowed the basin to develop at the cost of deforestation, pollution, and sedimentation. From the river's source in the Chambeshi region of Katanga to the Malebo Pool (also known as StanleyPool), the total length of the river is about 4200 km, with elevations varying between 300 and 1000 m. However, from the pool to the Atlantic Ocean, the flow distance is about 500 km, with a sharp 300 m gradient in elevation. Industrial activities and operations, such as open-pit artisanal mines and logging, continue to grow in the Congo. Fish is an important food source for the inhabitants of this basin, and about 20% of the population is engaged in fishing, roughly accounting for 61% of the total cash income. Hydropower potential amounting to about 100000 MW has been identified in the basin, but currently only less than 5 % of this potential is being exploited. The river network provides some 25000 km of navigable waterways, thus offering an opportunity for human mobility and exchange of goods and services between the riparian countries in such a humid tropical environment where maintenance of road infrastructure has always been a challenge.

2.2 Hydroclimate

Precipitation is highest in the central basins of the Congo River (the Upper Democratic Republic of Congo), and precipitation is lowest in the southeastern portion of the basin. The average annual precipitation is 1527 mm (Bultot, 1971), and the dual seasonal peaks occur in the Congo River discharge at Kinshasa station. The interannual variability ranges from a maximum of 1610 mm during the wettest decade of 1961–1970 to a minimum of 1515 mm during the driest decade of 1981–1989 (Mahé, 1995). A weak relationship is observed between rainfall and the sea surface temperature (SST) of the Pacific and the tropical Atlantic (Nicholson et al., 1997). The decrease in rainfall after the 1970s is smaller on

the east and southeast portions of the basin than in other regions of the river basin, and it is a result of the Atlantic monsoonal flow rather than of the air masses that carry moisture from the Indian Ocean (Tshitenge et al., 2015).

The mean annual temperature is 24.7 ℃, and the northern regions experience higher temperatures than the central or southern regions, while the southeastern region has the lowest temperature. The annual average daily maximum, mean, and minimum temperatures for major portions of the Congo Basin are 30 to 31 ℃, 23 to 25 ℃, and 18 to 20 ℃, respectively (Bultot, 1972). For the northern portions, the annual average temperatures between the 1950s and 1990s have increased from 0.4 to 1.0 ℃. For DRC, Kazadi and Kaoru (1996) also found increasing temperatures from 1960 to 1990 from 0.60 ℃/30 yr to 1.62 ℃/30 yr. Anomalous warm conditions over the Congo are more likely to be observed from 2 to 8 months after the initiation of El Niño over the Pacific Ocean. The temperature also follows the precipitation cycle, with the lowest temperature between June and August. The annual mean temperatures have increased from 1967 to 2012 (Figure 2).

Actual evapotranspiration (ET) varies from 800 mm in Katanga to 1200 mm in the Uele region (Eastern area of the Qubangui basin). For the entire Congo Basin, the actual ET is the major sink term, which is estimated to be about 75%-85% of the annual precipitation (Alsdorf et al., 2016). Nicholson et al. (1997) reported annually averaged potential ET peaks of about 1500 mm/yr near the equator, decreasing northward and southward to less than 1000 mm/yr. It is also reported that ET more than doubled in 1957 with the smallest values in February and the largest in September (Brutsaert, 1965). In addition, the values of potential evapotranspiration (PET) observed at Bangui and Brazzaville were highest in March–April and lowest in July (Riou, 1984).

The main stem of the Congo River has an annual discharge of 40,662 m^3/s from 2001 to 2010 (GRDC, 2020). Laraque et al. (2013) noted variations in the Congo River discharge varied between 1960 and 1995, and is only now returning to its long-term average . For Brazzaville, the period 1960–1970 saw a 21% increase, 1971–1981 had a 4.5% increase, and 1982–1993 saw a decrease of 5.3% in discharge as compared with the average between 1902 and 1959. Annual-average low flows of the Congo River are about 30,000 m^3/s and high flows about 55,000 m^3/s. Runge and Nguimalet (2005) determined that floods with a 2-year return period have a peak discharge of about 9800 m^3/s, whereas the 100-year flood has a peak magnitude of 15,800 m^3/s. Also, the maximum discharge values decreased after the 1960s and remained low until the 1990s. Hydrologically, residence time is important for the planning and management of water resources. It takes approximately 2 months for the flow to travel from the confluence of the Lualaba and Elila Rivers to Brazzaville, 1 month from the confluence of the Kotto and Oubangui Rivers, and about 15 days from the confluence of the Loange and Kasai Rivers. In the early 1900s, the April–May peaks appear more pronounced compared with the April–May peaks of the 2000s. Syed et al. (2009) used GRACE data from 2003 to 2006 to estimate terrestrial water storage changes and used precipitation and evapotranspiration (P-E) data from the National Centers for Environmental Prediction (NCEP) and the European Center for Medium-Range Weather Forecasting (ECMWF). Although there was, on average, general agreement in estimating the changes in storage, differences of up to 100 km^3 in October were evident.

Tshimanga and Hughes (2011), Tshimanga et al. (2012), and Tshimanga and Hughes (2014) assessed the performance a semi-distributed rainfall-runoff model and a number of inputs from global data sets, e.g., topography, vegetation, and soils. The results revealed that precipitation in the Congo was up to 40% less when compared with that in the Amazon River Basin, while ET was only 10% less. Water vapor that was transpired back to the atmosphere was 78% for the Congo compared with 62% for the Amazon.

Although the annually averaged discharge is about 5 times smaller in the Congo River than in the Amazon River, its basin area is half that of the Amazon Basin. Unlike the Amazon, which has a single-peak flow period, the Congo mainstem has two peak flow seasons per year. Storage changes in the mainstem Amazon floodplain are a function of both water levels and inundated area, whereas changes in the Congo Basin are determined by the Cuvette depression and the flooded areas in it.

2.3 Land cover change

Comparisons of the land-use and land cover distribution in the Congo River Basin for the years 1992 and 2015 derived from the annual European Space Agency Climate Change Initiative (ESA-CCI) land cover maps at a 300 m spatial resolution showed changes in some land cover types (Figure 3). The basin exhibits high variability in land-use and land cover types, with 37 original land cover classes based on the United Nations Land Cover Classification System. To assess the changes in major land cover types, this system was reclassified into 10 classes using the International Geosphere–Biosphere Programme (IGBP) scheme. Evergreen broadleaf forests occupied more than 40% of the basin and dominated in Middle Congo, Ruki, Yangambi, Sangha, Kinshasa, and Matadi subbasins. Also, croplands were present in Middle Congo, Ruki, Yangambi, Sangha, and Kinshasa subbasins. Deciduous forests were present mainly in Kasai, Upper Congo, Tanganyika, and Oubangui subbasins. In total, more than 80% of the Congo Basin was covered by forest. Lake Tanganyika is present in the southeastern part of the basin, with a surface area accounting for more than 1.5% of the basin area. The western region and eastern border areas included some anthropogenic activities, with areas covered by cropland (9.9%), bare soil (2.2%), and shrublands (2.8%). Croplands were also sparsely distributed in the Middle Congo. More specifically, the intensification of the anthropogenic activities is evident from the decrease in forest area by 746 km^2, the

157 decrease in natural vegetation by 30,000 km^2, the increase in urban area by 883 km^2, and the increase in
158 cropland by 3866 km^2 between 1992–2003 and 2004–2015 (Figure 4).

159 Specifically, a large deforestation pattern has been reported for all of the rainforests in the Middle
160 Congo and Qubangui regions between 1990 to 2010 (De Wasseige et al., 2009; De Wasseige et al.,
161 2014). In the Middle Congo region, there were decreases in tree cover (-2.2%) and grassland (-47.9%),
162 and increases in cropland (+13.3%) and Urban areas (94.4%) between 1992 to 2012. Besides, there were
163 increases in cropland (+17.6%) and Urban areas (42.5%), and decrease in Shrubland (-68.5%) in the
164 Qubangui region. (Figure 5 and Table 1). We estimated the impacts of those land cover changes on
165 hydrology by separate simulations using the two land cover data (1992 and 2012).

166 **3. Methods**

167 ***3.1. Hydrological Models***

168 In this study, we used a hydrological model for the water budget estimations and drought
169 evaluations. The soil and water assessment tool (SWAT) (Arnold et al., 1998, 2012) is a continuous, semi-
170 distributed, basin-scale, and hydrological model. The SWAT model is based on a hydrologic response
171 unit (HRU), which is a combination of land-use, soil, and slope properties of the watersheds. The SWAT
172 model have been widely applied to many river basins around the globe for drought assessments (Kang &
173 Sridhar, 2018a), water resource management, hydrologic response (Aloysius & Saiers, 2017), and water
174 budget estimations under historical and future climate conditions (Sridhar et al., 2019). For the Congo
175 River Basin, a 0.5-degree resolution of atmospheric forcing (daily precipitation, maximum and minimum
176 temperatures, and wind speed) from Sheffield et al. (2006) was applied, and 1,333 climate grids were
177 available. In order to consider all climate grids, the SWAT model was delineated at 1,732 sub-
178 watersheds.

17

18

179 The SWAT model requires a digital elevation model (DEM), soil data, and land-use data. The Shuttle
180 Radar Topography Mission 30 (SRTM30; 1 km resolution; Becker et al., 2009) was used as a DEM, and
181 the soil properties were obtained from the data set of the Food and Agriculture Organization of the
182 United Nations (FAO, 1995). In addition, the 300-meter resolution of land cover from ESA-CCI (ESA,
183 2014) was extracted for the Congo River Basin.

184 **3.2. *Drought Index***

185 The modified Palmer drought severity index (MPDSI; Mo & Chelliah, 2006) was used for the
186 historical and future drought assessments. MPDSI was developed to supplement the shortcomings of
187 the Palmer drought severity index (PDSI), including the estimation of PET with the Thornthwaite (1948)
188 formula. MPDSI is based on water budget principles between the climatological and actual precipitation
189 known as "climatically appropriate for existing conditions (CAFEC)," which is described in Equations 1
190 and 2.

191 $$CAFEC = \alpha PE + \beta PR + \gamma PRO + \delta PL \quad (1)$$

192 $$d = P - CAFEC \quad (2)$$

193 where PE is the potential evapotranspiration, PR is the potential recharge, PRO is the potential runoff,
194 and PL is the potential soil moisture loss. Further, α, β, γ, and δ are the ratios of the mean values of the
195 actual and potential water budget components over the simulation period. For example, α is the ratio of

196 actual and potential ET ($\alpha = \frac{\overline{ET}}{\overline{PET}}$). More detailed explanations are available from Mo and Chelliah
197 (2006). The monthly MPDSI was computed for each sub-watershed using the inputs and outputs of the
198 SWAT model, such as precipitation, PET, ET, runoff, baseflow, and soil moisture.

19

20

3.3. Climate Models

In this analysis, four global circulation models (GCMs) from two Representative Concentration Pathways (RCPs), 4.5 and 8.5, were used for future meteorological parameters, which are GFDL-ESM2M, IPSL-CM5A-LR, MIROC-ESM-CHEM, and NorESM1-M. The four climate models were chosen due to their wide ranges of wet/dry and cold/hot climate conditions defined using the precipitation and temperature changes between 2020 and 2099. The meteorological parameters of the GCMs were bias corrected and statistically downscaled to a 0.5-degree resolution using the Intersectoral Impact Model Intercomparison Project (ISI-MIP) approach (Hempel et al., 2013). Since the future period temperature was higher for all the GCMs with respect to the historical period, the cool climate scenario was not analyzed. The impact of climate change on the hydrological characteristics of the basin was well captured by the wide range of temperature (1.4 – 3.2 ℃) and precipitation (-7.2% - +21.3%) changes exhibited by the climate models. The change in the meteorological parameters was considerable for RCP8.5 as compared with RCP4.5, with the hottest and wettest scenarios exhibited by IPSL-CMA-LR and the driest climate conditions shown by NorESM1-M (Figure 6).

Compared with the historical period of 1956-2019, with a mean daily precipitation average of 3.99 mm/day, a modest increase in precipitation was expected in the future between 2020 and 2099; these increases were 4.10 mm/day for RCP 4.5 and 4.36 mm/day for RCP 8.5. IPSL-CM5A-LR showed the highest increase in precipitation under RCP4.5 and RCP8.5 in the eastern region. MIROC-ESM-CHEM showed a precipitation decline in the western region. An increase in monthly precipitation for all the months except September and October was seen under RCP4.5 and RCP8.5. The mean annual precipitation for the historical period is 1456 mm, while for the future period the precipitations are 1497 and 1592 mm under RCP4.5 and RCP8.5, respectively. The mean annual temperature for the historical

period was 24.7 ℃, while for the future period the temperatures were estimated to be about 26.3 and 27.5 ℃ under RCP4.5 and RCP8.5, respectively. The average increases in monthly temperature of 1.6 and 2.7 ℃ were projected between now and the end of the century for RCP4.5 and RCP8.5, respectively. The highest increase is predicted for July (Figure 7).

3.4. GRACE Satellite TWSA

The terrestrial water storage anomaly (TWSA) was estimated for the hydrological analysis of the study area using the water budget framework. The net water balance resulting from the accumulation of water entering the upper section of the soil column through rainfall and adjacent soil units and the reduction due to evapotranspiration and runoff was calculated by water budget accounting. Mathematically, the mass conservation equation for the terrestrial water storage change (TWSC) is as follows:

$$TWSC = P - ET + R_{¿} - R_{out} \quad (3)$$

where P is precipitation, ET is evapotranspiration, $R_{¿}$ is water entering from adjacent soil, and R_{out} is runoff exiting the soil column. The groundwater flux contribution to the storage change was assumed to be negligible (Syed et al., 2008). The SWAT model were used for the derivation of precipitation, evapotranspiration, and runoff to estimate storage change. The simulated TWSC was compared with the remotely sensed production, GRACE-derived TWSC for the period between 2002 and 2016. The TWSA from the GRACE data set is available at a 1-month temporal and 1-degree spatial resolution from the Jet Propulsion Laboratory (JPL) for the interpretation of water storage change (Swenson & Wahr, 2006). In order to minimize the smoothed and unfiltered monthly water variation differences and account for the heterogeneity in the water budget components across the domain, the grid scaling factor is multiplied with the GRACE TWSA (Wiese et al., 2016). The monthly GRACE TWSA product supported the estimation

of the TWSC calculation as the difference between two consecutive time steps. The relationship between the TWSC and the TWSA can be written as

$$TWSC\,GRACE(\Delta t) = TWSA_{(t_i+\Delta t)} - TWSA_{(t_i)} \quad (4)$$

where $t_i + \Delta t$ and t_i are the ending and starting times, respectively, with a time step duration of Δt.

4. Results and Discussion

4.1. Model Evaluation and impacts of land cover changes

The calibration of the hydrological models was performed by comparing the monthly simulated streamflow with the observed streamflow at seven gage stations distributed across the basin—namely, Chembe Ferry, Kasongo Lualaba, Ilebo, Ouesso Sangha, Bangui Oubangui, Kutu Moke Kasai, Kinshasa — (Figure 1 and Table 2). The SWAT captured the interannual variability in the annual hydrographs for all the sites. The Nash–Sutcliffe model efficiency coefficient (NS; Nash & Sutcliffe, 1970) and the coefficient of determination (r^2) were estimated to evaluate the ability of the SWAT model to simulate the observed streamflow. The validation process was performed only some stations where the continuous and long-term observations are available (more than 20 years). The parameters used for the calibration and validation of the SWAT model are presented in Table 3, respectively. The NS values from the SWAT model during the calibration and validation periods are presented in Table 2. The NSE values were above to 0.65 for all stations, which were assumed to be “good” or “very good” for the monthly simulations (Moriasi et al., 2007; Seong & Sridhar, 2017). Based on the NS values, the SWAT model was able to capture the hydrologic responses of the Congo River Basin to changing environmental and biophysical conditions.

Using the calibrated parameters, impacts of land cover changes on hydrology were evaluated for a simulation period of 30 years with the two separate land cover data (1992 and 2012). Figure 8 presents the results of the water budgets and streamflow. Figure 8a is the ET averaged over 30 years, Figure 8b shows the average soil moisture, and Figure 8c compares the monthly average flow from the simulations of two land covers. During the twenty years, there were overall decreases in tree cover, shrubland, and grassland areas, and agricultural and urban areas increased significantly. These changes resulted in ET decreases, reductions in storage capacity that led to a soil moisture decrease, ultimately in streamflow increases. For the Qubangui and Middle Congo regions, there were 12.2% and 16.2% increases in streamflow, respectively. If the forest losses and urbanization are continually proceeding in the future, the flow increases would lead to flooding and agricultural drought increases due to a decrease in soil moisture. In this study, the irrigation amount or reservoir impacts were not considered, thus the result was mainly based on natural flow and water budgets.

4.2. Total Water Storage Analysis

Spatial maps of TWSC from GRACE-satellite observations and the SWAT model for 2006 are presented in Figure 9. The model-derived TWSC was computed by the mass conservation equation of change in water storage (Equation 3). The GRACE-derived TWSC was calculated by the difference between GRACE TWSA at two different time steps (Equation 4). Overall, the results implied that the spatiotemporal trends of the model-derived TWSCs were similar to the trend of the GRACE-derived TWSC. Although this analysis is carried out for a 10-year period between 2002 and 2012, the spatial illustration of comparisons is shown for one year only, and the time series of domain averages are presented in the following section. GRACE detected drier conditions in the northwestern region of the basin between January and April. The upstream portions of the basin began to exhibit deficit moisture conditions in May and remained relatively dry through October. This pattern was consistent for all the study periods. For the remaining period between November and April, the central and southern regions were relatively wet.

Figure 10 illustrates the time-averaged seasonal TWSC, and GRACE-estimated TWSC was used to compare the SWAT-simulated TWSC for the basin. It was evident that the SWAT model closely matched the monthly averaged values. Compared to the GRACE TWSC, the SWAT model resulted in wetter conditions from August to April, and drier conditions from May to July. This analysis was conducted by averaging at the basin scale, and the model results can be used as a baseline condition to estimate the changes in terrestrial water storage; however, subbasin-scale analysis would be required for better results. There were significant spatial and temporal mismatches during September and October, and the model-driven TWSC showed faster recovery from the negative conditions. Besides, model-driven TWSC

showed higher variabilities compared to GRACE-based TWSC. The differences might be derived that the spatial resolution of the GRACE-derived TWSC was 1°, and that of the model-derived TWSC was 0.5°.

4.3. Historical Changes in Water Budgets and Drought Occurrences

Time series analysis of TWSA and MPDSI is shown in Figure 11. There is a strong correlation between TWSA and MPDSI. Clearly, the wetter conditions with positive anomalies and the drier basin with negative anomalies were seen for the 10-year correlation analysis, and the results verified that lower TWSA represents moisture deficit that leads to higher drought severities. In contrast, higher TWSA indicates surplus moisture conditions, which result in lower drought severities. The average change in TWSA for the basin was -0.14 cm. The patterns reflected the rainfall variability from year to year, which was closely captured by both TWSA and MPDSI. The years 2006 and 2011 were the driest during the study period, and they were captured by both TWSA and MPDSI. Interestingly, the bimodal TWSA demonstrated the two precipitation peaks that the basin received (Figure 11a). With a coefficient of determination (r^2) of 0.65, a tight correlation was also evident. In other words, the model-derived soil moisture that was used to calculate MPDSI demonstrated the capability of this approach to draw basin-scale inferences on water availability and drought conditions (Figure 11b). Satellite data and a hydrological model can complement each other in mapping drought-hit areas and water-stressed regions for this basin. Especially in the basin's rainforests, which are critical for both local and global climate, understanding the length of the dry season and sustaining the rainforests as shown with TWSA and MPDSI can be of added value in managing the basin's water resources. The dry season in the Congo River Bain was from April to August, which includes the pre-dry season (April to June) (Hua et al., 2016). Also, it was reported that dry season length had increased by 6.4 – 10.4 days per decade due to large-scale decreases in forest greenness and canopy water content (Jiang et al., 2019). Thus, a reliable

320 estimation of water storage during the dry season is essential, and the results of model-driven drought
321 index and TWSA can be appropriately implemented to understand the dry season in the Congo basin.

322 To assess the accuracy of the model-driven drought index (MPDSI), we compared MPDSI and PDSI
323 derived by Dai et al. (2011), which was used for a reference drought index. Model-derived MPDSI
324 showed a good temporal agreement with PDSI between 1950 and 1999 (Figure 12a). High values of the
325 early 1960s and low values of the late 1990s and the interannual variability in drought occurrences
326 corresponded well between PDSI and MPDSI, with an r^2 of 0.59. Like that of PDSI, the calculation
327 method of MPDSI also considered CAFEC, which stands for climatologically expected precipitation over
328 the maximum conditions. In addition, SWAT-estimated ET, PET, soil moisture, and runoff were used for
329 the MPDSI calculation. Palmer (1965) assumed that potential precipitation is equivalent to available
330 water capacity, despite there being no significant relationship between them and no direct use of soil
331 moisture in the calculation. Therefore, MPDSI estimation seemed appropriate for this region. Because
332 of the physical differences in estimating PDSI and MPDSI, the dry-down phase was different between
333 them. In other words, MPDSI retained more moisture within the soil column than PDSI, and the extent
334 of drought severity was less and more realistic with MPDSI than with PDSI. Generally, PDSI overpredicts
335 drought when ET is computed by the Thornthwaite method as it is highly sensitive to temperature
336 changes. The mean values of MPDSI for each month (January to December) are shown in Figure 12b,
337 which represent the averages of two periods (1913–1962 and 1962–2012). Qubangui (northern areas of
338 the basin) and Middle Congo regions showed increases in drought severity (Figure 12b) and occurrence
339 (Figure 12c) during the second period (1962–2012), driven by the decrease in precipitation exhibited in
340 the orange to red areas in Figure 12d.

341 ***4.4. Impacts of Climate Change on Droughts and Water Budgets***

33

34

Figures 13a and 13b present the time series of MPDSI for historical and future periods. The historical mean was 0.92, but the future mean values of RCP4.5 and RCP8.5 were 0.73 and 0.90, respectively. Increases in future drought severities and occurrences are expected, with less negative MPDSI values in both scenarios. However, the basin was projected to have interannual variability in drought conditions, and the uncertainties captured with the shaded areas in the time series suggested that precipitation, temperature, and soil moisture estimation based on assumed vegetation played a major role. In addition, the average values of maximum and minimum were 1.72 and -0.21 for RCP4.5, and 1.95 and -0.15 for RCP8.5. The results of RCP8.5 showed a higher range of uncertainties.

Figure 13c shows MPDSI differences between historical and future periods, and they were calculated by the subtraction of average MPDSI values between historical and future periods (future MPDSI – historical MPDSI). A combination of precipitation decreases (or relatively lower increases—less than 2%) and temperature increases of up to 3 °C are found to have an impact on the increases in drought severities under future climate change conditions in the Congo River Basin (Figure 13c). Future increases in temperature led to an increase of up to 11% in ET simulated by the SWAT model (Figure 13a), and this might be causing increases in projected drought conditions.

4.5 Water Budget Changes

Figure 14a presents the spatial maps of changes in ET and runoff between historical and future periods from the SWAT model, and Figure 14b shows the bar charts of changes in ET and runoff for each subbasin. Changes were the percentage increases or decreases in the future period (2020–2099) relative to the historical period (1956–2019). ET and runoff changes were calculated for each subregion in the Congo River Basin. For both RCP4.5 and RCP8.5, there were increases in ET of up to 9% and runoff changes between -1% and 53%. Water budget changes were highly influenced by precipitation and

364 temperature alterations in the sub-basins. For instance, there were overall ET and runoff increases for
365 the middle and upper areas as projected by both models, and these were the regions where overall
366 precipitation and temperature increases were expected. The runoff estimations of the SWAT model
367 were sensitive to the precipitation changes and the curve number values. For instance, in the Middle
368 Congo region, the SWAT model estimated runoff increase between 27% and 53% for RCP4.5 and RCP8.5.

369

370 **5. Conclusions**

371 The Congo Basin is a relatively large and underdeveloped region. The basin is experiencing longer
372 dry seasons, and this is expected to impact water resources and drought. Using an established
373 hydrological model, we have simulated water budget components, including streamflow, soil moisture,
374 and evapotranspiration, using past and future climate conditions to aid in the understanding of the
375 drought characteristics in this region, where in situ data are scarce. Major portions of the Congo River
376 Basin normally have two peak flow seasons per year, and the flow changes in the Congo River Basin are
377 also substantially influenced by the Cuvette depression and the flooded areas within this region. We
378 evaluated the land-use and land cover distribution in the Congo River Basin for the years 1992 and 2012
379 and found that forests and native vegetation decreased over this period while urban and cropland areas
380 showed marginal increases. However, hydrological changes (streamflow, soil moisture,
381 evapotranspiration) due to land cover changes were within the margin of the hydrological models'
382 uncertainties, and they were considered minimal. The major findings of this study are the following:

383 • Hydroclimate assessment of total water storage conditions integrated with hydrological
384 models and remote sensing demonstrated the feasibility of such a framework in the Congo
385 River Basin.

37

38

- There were huge decreases in forest and shrubland, and increases in urban areas in the Qubangui and Middle Congo regions, and those changes led to dramatic water budget alterations and streamflow increases.
- Basin-scale variability in temperature and precipitation has impacted streamflow and exacerbated TWSA conditions. The use of GRACE to assess water availability was proven to be beneficial and demonstrates the potential when it is available to benefit local-scale analysis.
- A soil-moisture-based drought index such as MPDSI can be effective when temperature and precipitation have a significant impact on the water budget.
- Future temperature increase and spatially variable precipitation will contribute to subbasin-scale differences with different magnitudes of change, but in general, increased ET and runoff, and more drought events were projected in the basin.

References

Ali, S. A., & Sridhar, V. (2019). Deriving the Reservoir Conditions for Better Water Resource Management Using Satellite-Based Earth Observations in the Lower Mekong River Basin. Remote Sensing, 11(23), 2872. https://doi.org/10.3390/rs11232872

Aloysius, N., & Saiers, J. (2017). Simulated hydrologic response to projected changes in precipitation, Hydrol. Earth Syst. Sci., 21, 4115–4130, 2017.

Arnold, J. G., Srinivasan, R., Muttiah, R. S., & Williams, J. R. (1998). Large area hydrologic modeling and assessment part I: model development. Journal of the American Water Resources Association, 34(1), 73–89. https://doi.org/10.1111/j.1752-1688.1998.tb05961.x

Arnold, J. G., Moriasi, D. N., Gassman, P. W., Abbaspour, K. C., White, M. J., Griensven, V., & Liew, V. (2012). SWAT: Model use, calibration, and validation. Transactions of the ASABE, 55(4), 1491–1508. Retrieved from https://digitalcommons.unl.edu/biosysengfacpub/406

Becker, J. J., Sandwell, D. T., Smith, W. H. F., Braud, J., Binder, B., Depner, J., et al. (2009). Global Bathymetry and Elevation Data at 30 Arc Seconds Resolution: SRTM30 PLUS. Marine Geodesy, 32(4), 355–371. https://doi.org/10.1080/01490410903297766

Bisht, D. S., Chatterjee, C., Raghuwanshi, N. S., & Sridhar, V. (2018). Spatio-temporal trends of rainfall across Indian river basins. Theoretical and Applied Climatology, 132(1–2), 419–436. https://doi.org/10.1007/s00704-017-2095-8

Brutsaert, W. (1965). Evaluation of some practical methods of estimating evapotranspiration in arid climates at low latitudes. Water Resources Research, 1(2), 187-191.

Bultot, F. (1971). Atlas Climatique du Bassin Congolais Publications de L'Institut National pour L'Etude Agronomique du Congo (I.N.E.A.C.), Deuxieme Partie, Les Composantes du Bilan d'Eau.

Bultot, F. (1972). Atlas Climatique du Bassin Congolais Publications de L'Institut National pour L'Etude Agronomique du Congo (I.N.E.A.C.), Troisieme Partie, Temperature et Humidite de L'Air, Rosee, Temperature du Sol.

Cosby, B. J., Hornberger, G. M., Clapp, R. B., & Ginn, T. R. (1984). A Statistical Exploration of the Relationships of Soil Moisture Characteristics to the Physical Properties of Soils. Water Resources Research, 20(6), 682–690. https://doi.org/10.1029/WR020i006p00682

Dai, A. (2011). Characteristics and trends in various forms of the Palmer Drought Severity Index during 1900–2008. Journal of Geophysical Research, 116(D12), D12115. https://doi.org/10.1029/2010JD015541

De Wasseige, C., Devers, D., de Marcken, P., Ebaa Atyi, R., Nasi, R., & Mayaux, P. (2009). Les forêts du Bassin du Congo- État des Forêts 2008. Office des publications officielles des Communautés européennes 425 p.

De Wasseige, C., Flynn, J., Louppe, D., Hiol Hiol, F. & Mayaux, P. (2014). The Forests of the Congo Basin-State of the Forest 2013. Weyrich.

ESA. (2014). CCI Land Cover Product User Guide version2.4. ESA CCI LC Project.

FAO. (1995). Digital Soil Map of the World and Derived Soil Properties. Food and Agriculture Organization of the United Nations, Rome.

Global Runoff Data Center (GRDC) (2020), [Available at http://www.bafg.de/GRDC/EN/Home/homepage_node.html (last accessed July 30, 2020).]

Hempel, S., Frieler, K., Warszawski, L., Schewe, J., & Piontek, F. (2013). A trend-preserving bias correction – the ISI-MIP approach. Earth System Dynamics, 4(2), 219–236. https://doi.org/10.5194/esd-4-219-2013

Hoekema, D. J., & Sridhar, V. (2013). A System Dynamics Model for Conjunctive Management of Water Resources in the Snake River Basin. JAWRA Journal of the American Water Resources Association, 49(6), 1327–1350. https://doi.org/10.1111/jawr.12092

Jaksa, W. T., & Sridhar, V. (2015). Effect of irrigation in simulating long-term evapotranspiration climatology in a human-dominated river basin system. Agricultural and Forest Meteorology, 200, 109–118. https://doi.org/10.1016/j.agrformet.2014.09.008

Jiang, Y., Zhou, L., Tucker, C. J., Raghavendra, A., Hua, W., Liu, Y. Y., & Joiner, J. (2019). Widespread increase of boreal summer dry season length over the Congo rainforest. Nature Climate Change, 9(8), 617–622. https://doi.org/10.1038/s41558-019-0512-y

Kang, H., & Sridhar, V. (2017). Combined statistical and spatially distributed hydrological model for evaluating future drought indices in Virginia. Journal of Hydrology: Regional Studies, 12, 253–272. https://doi.org/10.1016/J.EJRH.2017.06.003

Kang, H., & Sridhar, V. (2018a). Assessment of Future Drought Conditions in the Chesapeake Bay Watershed. Journal of the American Water Resources Association, 54(1), 160–183. https://doi.org/10.1111/1752-1688.12600

Kang, H., & Sridhar, V. (2018b). Improved Drought Prediction Using Near Real-Time Climate Forecasts and Simulated Hydrologic Conditions. Sustainability, 10(6), 1799. https://doi.org/10.3390/su10061799

Kazadi, S. N., & Kaoru, F. (1996). Interannual and long-term climate variability over the Zaire River Basin during the last 30 years. Journal of Geophysical Research Atmospheres, 101(16), 21351–21360. https://doi.org/10.1029/96jd01869

Laraque, A., Bellanger, M., Adèle, G., Guebanda, S., Gulemvuga, G., Pandi, A., Paturel, J.E., Robert, A., Tathy, J.P. & Yambele, A. (2013). Recent evolution of the Congo, Oubangui and Sangha River flows. Acad. R. Sci. Bel., Geo-Eco-Trop, 37(1), 93-100.

Liang, X., Lettenmaier, D. P., Wood, E. F., & Burges, S. J. (1994). A simple hydrologically based model of land surface water and energy fluxes for general circulation models. Journal of Geophysical Research, 99(D7), 14415. https://doi.org/10.1029/94JD00483

Mahé, G. (1995). Modulation annuelle et fluctuations interannuelles des précipitations sur le bassin-versant du Congo, in Actes du Colloque PEGI Grands Bassins Fluviaux Péri-Atlantiques, edited by J. Boulègue and J. C. Olivry, pp. 13–26Congo, Niger, Amazone, INSU, CNRS, ORSTOM, Paris.

Mishra, V., Shah, R., Azhar, S., Shah, H., Modi, P., & Kumar, R. (2017). Reconstruction of droughts in India using multiple land surface models (1951–2015). Hydrology and Earth System Sciences Discussions, 1–22. https://doi.org/10.5194/hess-2017-302

Mo, K. C., & Chelliah, M. (2006). The modified Palmer drought severity index based on the NCEP North American Regional Reanalysis. Journal of Applied Meteorology and Climatology, 45(10), 1362–1375.

Moriasi, D. N., Arnold, J. G., Liew, M. W. Van, Bingner, R. L., Harmel, R. D., & Veith, T. L. (2007). Model evaluation guidelines for systematic quantification of accuracy in watershed simulations. Transactions of the ASABE, 50(3), 885–900.

Nash, J. E., & Sutcliffe, J. V. (1970). River flow forecasting through conceptual models part I — A discussion of principles. Journal of Hydrology, 10(3), 282–290. https://doi.org/10.1016/0022-1694(70)90255-6

Palmer, W. (1965). Meteorological drought (Vol. 30). US Department of Commerce, Weather Bureau. Retrieved from https://books.google.com/books?hl=en&lr=&id=kyYZgnEk-L8C&oi=fnd&pg=PR2&dq=Palmer+(1965)+&ots=U3guah1Flp&sig=2FsxCwGPJCzise2CQ4I4b-TATqQ

Riou, C. (1984). Experimental study of potential evapotranspiration (PET) in Central Africa. Journal of hydrology, 72(3-4), 275-288.

Runge, J. (2007). The Congo River, Central Africa. In Large Rivers: Geomorphology and Management (pp. 293–309). Chichester, UK: Wiley Blackwell. https://doi.org/10.1002/9780470723722.ch14

Runge, J., & Nguimalet, C. R. (2005). Physiogeographic features of the Oubangui catchment and environmental trends reflected in discharge and floods at Bangui 1911-1999, Central African Republic. Geomorphology, 70(3-4 SPEC. ISS.), 311–324. https://doi.org/10.1016/j.geomorph.2005.02.010

Sehgal, V., & Sridhar, V. (2018). Effect of hydroclimatological teleconnections on the watershed-scale drought predictability in the southeastern United States. International Journal of Climatology, 38, e1139–e1157. https://doi.org/10.1002/joc.5439

Seong, C., & Sridhar, V. (2017). Hydroclimatic variability and change in the Chesapeake Bay Watershed. Journal of Water and Climate Change, 8(2), 254–273. https://doi.org/10.2166/wcc.2016.008

Sheffield, J., Goteti, G., & Wood, E. F. (2006). Development of a 50-Year High-Resolution Global Dataset of Meteorological Forcings for Land Surface Modeling. Journal of Climate, 19(13), 3088–3111. https://doi.org/10.1175/JCLI3790.1

Sridhar, V., & Anderson, K. A. (2017). Human-induced modifications to land surface fluxes and their implications on water management under past and future climate change conditions. Agricultural and Forest Meteorology, 234–235, 66–79. https://doi.org/10.1016/j.agrformet.2016.12.009

Sridhar, V., Jin, X., & Jaksa, W. T. A. (2013). Explaining the hydroclimatic variability and change in the Salmon River basin. Climate Dynamics, 40(7–8), 1921–1937. https://doi.org/10.1007/s00382-012-1467-0

Sridhar, V., Ali, S. A., & Lakshmi, V. (2019). Assessment and validation of total water storage in the Chesapeake Bay watershed using GRACE. Journal of Hydrology: Regional Studies, 24, 100607. https://doi.org/10.1016/J.EJRH.2019.100607

Sridhar, V., Kang, H., & Ali, S. A. (2019). Human-Induced Alterations to Land Use and Climate and Their Responses for Hydrology and Water Management in the Mekong River Basin. Water, 11(6), 1307. https://doi.org/10.3390/w11061307

Swenson, S., & Wahr, J. (2006). Post-processing removal of correlated errors in GRACE data. Geophysical Research Letters, 33(8), L08402. https://doi.org/10.1029/2005GL025285

Syed, T. H., Famiglietti, J. S., & Chambers, D. P. (2009). GRACE-Based Estimates of Terrestrial Freshwater Discharge from Basin to Continental Scales. Journal of Hydrometeorology, 10(1), 22–40. https://doi.org/10.1175/2008JHM993.1

Syed, T.H., Famiglietti, J.S., Rodell, M., Chen, J. & Wilson, C.R., (2008). Analysis of terrestrial water storage changes from GRACE and GLDAS. Water Resources Research, 44(2).

Thilakarathne, M., & Sridhar, V. (2017). Characterization of future drought conditions in the Lower Mekong River Basin. Weather and Climate Extremes, 17, 47–58. https://doi.org/10.1016/J.WACE.2017.07.004

Thornthwaite, C. W. (1948). An approach toward a rational classification of climate. Geographical Review, 38(1), 55–94. Retrieved from https://www.jstor.org/stable/210739?casa_token=DENIJ_PuRskAAAAA:w1nhF0QBh9_y41VdaHHOQy4rAu2sBjRHId15A4U4vnLjKpOv5ZPHUi95HXo2MOHUuAW3DzNajq93M3oJM5kxX-KIRnbJZn8No64cb0QTZJBYMlDMHA

Tshimanga, R. M. (2012). Hydrological uncertainty analysis and scenario-based streamflow modelling for the Congo River Basin. Rhodes University. Retrieved from https://core.ac.uk/download/pdf/145042917.pdf

Tshimanga, R. M., & Hughes, D. A. (2014). Basin−scale performance of a semidistributed rainfall−runoff model for hydrological predictions and water resources assessment of large rivers: The Congo River. Water Resources Research, 50(2), 1174–1188. https://doi.org/10.1002/2013WR014310@10.1002/(ISSN)1944-7973.CHWREA1

Tshimanga, R. M., Hughes, D. A., & Kapangaziwiri, E. (2011). Initial calibration of a semi-distributed rainfall runoff model for the Congo River basin. Physics and Chemistry of the Earth, 36(14–15), 761–774. https://doi.org/10.1016/j.pce.2011.07.045

Tshitenge Mbuebue, J. M., Lukanda Mwamba, V., Tshimanga Muamba, R., Javaux, M., & Mahe, G., (2015). Wavelet Analysis on the Variability and the Teleconnectivity of the Rainfall of the Congo Basin for 1940–1999. In Conférence Internationale sur l'Hydrologie des Grands Bassins Africains.

Wiese, D. N., Landerer, F. W., & Watkins, M. M. (2016). Quantifying and reducing leakage errors in the JPL RL05M GRACE mascon solution. Water Resources Research, 52(9), 7490–7502. https://doi.org/10.1002/2016WR019344

List of Tables

List of Figures

Figure 6. Spatial variation in daily precipitation for historical (1950–2005) and future (2006–2099) periods in the Congo River Basin derived from GFDL-ESM2M, IPSL-CM5A-LR, MIROC-ESM-CHEM, and NorESM1-M global circulation models (GCMs) at a 0.5-degree spatial resolution. The percentage change in the precipitation for the future period under RCP4.5 and RCP8.5 with respect to the historical period is shown above. The seasonal variation in the precipitation is derived from the ensemble mean of the monthly values of the four GCMs for the historical and future periods. The annual fluctuation in the precipitation from 1950 to 2099 is extracted as the ensemble mean annual values of the four GCMs.

Figure 7. Spatial variation in the daily temperature for historical (1950–2005) and future (2006–2099) periods in the Congo River Basin derived from GFDL-ESM2M, IPSL-CM5A-LR, MIROC-ESM-CHEM, and NorESM1-M global circulation models (GCMs) at a 0.5-degree spatial resolution. The absolute change in the temperature for the future period under RCP4.5 and RCP8.5 with respect to the historical period is shown above. The seasonal variation in the temperature is derived from the ensemble mean of the monthly values of the four GCMs for the historical and future periods. The annual fluctuation in the temperature from 1950 to 2099 is extracted as the ensemble mean annual values of the four GCMs.

Figure 8. Results of land cover change analyses. (a) Spatial maps of ET derived by 30 years SWAT simulation (1983-2012) using 1992 and 2012 land cover maps. The red boxes highlight a region where the huge ET differences occur. (b) Spatial maps of soil moisture derived by 30 years of SWAT simulation (1983-2012) using 1992 and 2012 land cover maps. The red boxes highlight a region where the huge soil moisture differences occur. (c) Comparisons of monthly mean flow at the downstream stations of Qubangui and Middle Congo. Green lines indicate the results from the simulation with land cover 1992, while black lines represent the simulation with land cover 2012.

595 Figure 9. Spatial maps of terrestrial water storage change (TWSC) from GRACE satellite observations and
596 the SWAT and VIC models (results of 2006). The maps present the results of each month. Yellowish-
597 green to green areas indicate positive TWSC, while yellow to red areas present negative TWSC.
598 Figure 10. Variation in the ensemble mean of monthly total water storage change (TWSC) in the Congo
599 River Basin estimated from monthly GRACE mass grids and monthly SWAT-simulated water budget
600 components for the period 2002–2016.
601 Figure 11. Comparisons of total water storage anomalies (TWSAs) and MPDSI. (a) Time series of TWSA
602 and MPDSI. Green and blue lines present TWSA and MPDSI, respectively. (b) Scatter plot of TWSA and
603 MPDSI. X- and Y-axis represent TWSA and MPDSI, respectively.
604 Figure 12. Historical drought conditions in the Congo Basin. (a) Time series of model-estimated MPDSI
605 (red line) and PDSI (black line). (b) Seasonal comparisons of the mean values of MPDSI for each
606 subregion between two periods (P1:1913–1962, P2: 1963–2012). (c) Spatial maps of drought severity
607 based on the results of MPDSI between the two periods. The Figure 12c was calculated by the
608 subtraction of average MPDSI values from two periods (P1: 1913-1962, P2: 1963-2012) for each sub-
609 watershed. The negative values are symbolized as orange to red and they indicate the increases in
610 drought severity in the P2 period, while the positive values represent the decreases in drought severity
611 in the P2 period.
612 Figure 13. Historical drought conditions in the Congo Basin. (a, b) Time series of historical and future
613 MPDSI for the Congo Basin. The black lines indicate the mean values for the historical period, and the
614 red lines are the mean values for the future periods from the four climate models. The gray areas
615 indicate the range of climate models for the future periods. (a) and (b) present the results of RCP4.5 and
616 RCP8.5, respectively. (c) Spatial maps of drought severity based on the results of MPDSI between the
617 historical and future periods. The negative values are symbolized as orange to red and they indicate the

57
58

increases in drought severity in the future period, while the positive values represent the decreases in drought severity in the future period.

Figure 14. Water budget changes between historical (1956–2005) and future periods (2020–2099) under RCP4.5 and RCP8.5 simulated by the SWAT and VIC models. (a) Spatial maps of evapotranspiration (ET) and runoff changes. Orange to red colors indicate decreases in water budget, while green colors show increases. (b) Change in ET and runoff for the ten subregions. The change in ET and runoff was estimated as the ensemble mean derived from GFDL-ESM2M, IPSL-CM5A-LR, MIROC-ESM-CHEM, and NorESM1-M GCMs at a 0.5-degree spatial resolution. (c) Average of precipitation and temperature changes between historical (1956–2005) and future periods (2020–2099) under RCP4.5 and RCP8.5.

Table 1. Land use changes in the Qubangui and Middle Congo between 1992 and 2012

	Qubangui (km^2)			Middle Congo (km^2)		
	1992	2012	Change (%)	1992	2012	Change (%)
Cropland	16,542.5	19,460.4	17.6	44,087.4	49,935.4	13.3
Herbaceous	56,081.0	59,316.1	5.8	16,341.0	21,751.0	33.1
Tree cover	561,304.0	564,617.3	0.6	464,034.2	453,625.0	-2.2
Shrubland	12,523.2	3,946.3	-68.5	341.1	364.8	7.0
Natural vegetation	5,469.4	4,337.5	-20.7	6,043.7	4,892.6	-19.0
Grassland	2,174.0	2,146.1	-1.3	87.0	45.3	-47.9
Bare areas	6.8	13.3	94.4	49.4	54.2	9.9
Urban areas	130.0	185.2	42.5	112.9	219.6	94.4
Water bodies	2,911.0	3,119.6	7.2	4,942.7	5,151.3	4.2
Sum	657,141.9	657,141.9		536,039.3	536,039.3	

Table 2. The results of streamflow calibration and validation (NS, Nash and Sutcliffe efficiency coefficient (Nash and Sutcliffe, 1970), R^2: coefficient of determination)

Station name	Latitude	Longitude	Calibration period	Calibration		Validation period	Validation	
				NS	R^2		NS	R^2
Chembe Ferry	-11.97	28.76	1972-1981	0.81	0.82	-	-	-
Kasongo Lualaba	-4.53	26.58	1959-1968	0.72	0.73	-	-	-
Ilebo	-4.33	20.58	1981-1990	0.71	0.8	-	-	-
Ouesso Sangha	1.62	16.05	1960-1977	0.72	0.78	1978-1996	0.76	0.79
Bangui Oubangui	4.37	18.61	1960-1977	0.56	0.71	1978-1996	0.76	0.78
Kutu Moke Kasai	-3.18	17.38	1971-1980	0.65	0.76	1981-1990	0.76	0.85
Kinshasa Congo	-4.3	15.31	1995-2000	0.65	0.66	-	-	-

638 Table 3. Description of the SWAT parameters for the streamflow calibration.

Parameter	Description	Min	Max
R_CN2.mgt	Curve number for moisture condition II	-0.4	0.3
V_ALPHA_BF.gw	Base flow alpha factor	0	1
V_GW_DELAY.gw	Ground water delay time	30	400
V_GWQMN.gw	Threshold water Depth in shallow aquifer for back discharge	100	5000
V_ESCO.hru	Plant uptake compensation factor	0.01	1
V_EPCO.hru	Soil evaporation compensation factor	0.01	1
V_SLSUBBSN.hru	Average slop length	10	150
V_SURLAG.bsn	Surface runoff lag coefficient	1	24
V_REVAPMN.gw	Threshold depth of water in the shallow aquifer for "revap" to occur (mm)	0	500
V_GW_REVAP.gw	Groundwater "revap" coefficient	0.02	2
V_SOL_AWC.sol	Available water capacity of the soil layer	0	1
V_CH_K2.rte	Main channel conductivity	1	150
V_CH_N2.rte	Manning's n value for main channel	0	0.3
V_OV_N.hru	Manning's n value for overland flow	0	0.8
V_TIMP.bsn	Snow pack temperature lag factor	0	1
R_SOL_ZMX.sol	Maximum rooting depth of soil profile	-0.3	0.3
R_SOL_Z.sol	Depth from soil surface to bottom of layer	-0.3	0.3
R_SOL_K	Saturated hydraulic conductivity	-0.3	0.3
V_ALPHA_BNK	Baseflow alpha factor for bank storage	0	1
V_CANMX	Maximum canopy storage	0	100
R_HRU_SLP	Average slope steepness	-0.25	0.25

639

65

66

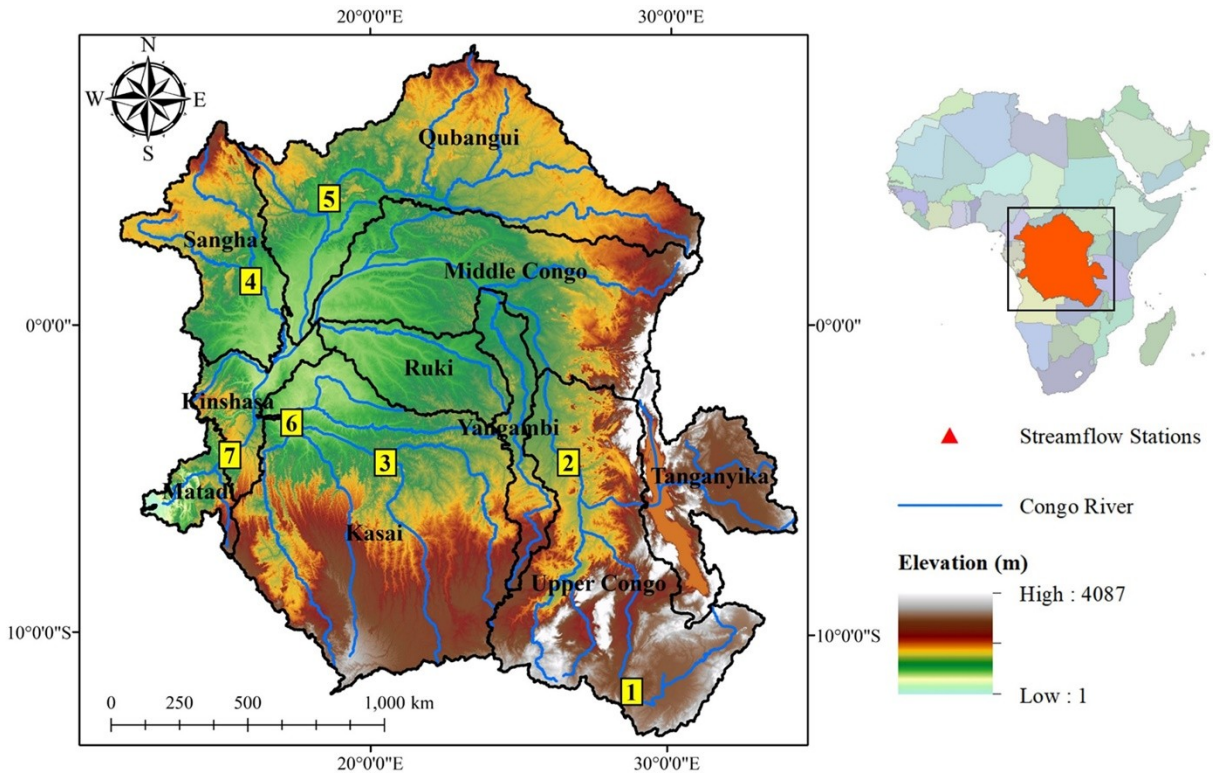

Streamflow stations

1. Chembe Ferry, 2. Kasongo Lualaba, 3. Ilebo, 4. Ouesso Sangha, 5. Bangui Oubangui, 6. Kutu Moke Kasai, 7. Kinshasa

Figure 1.

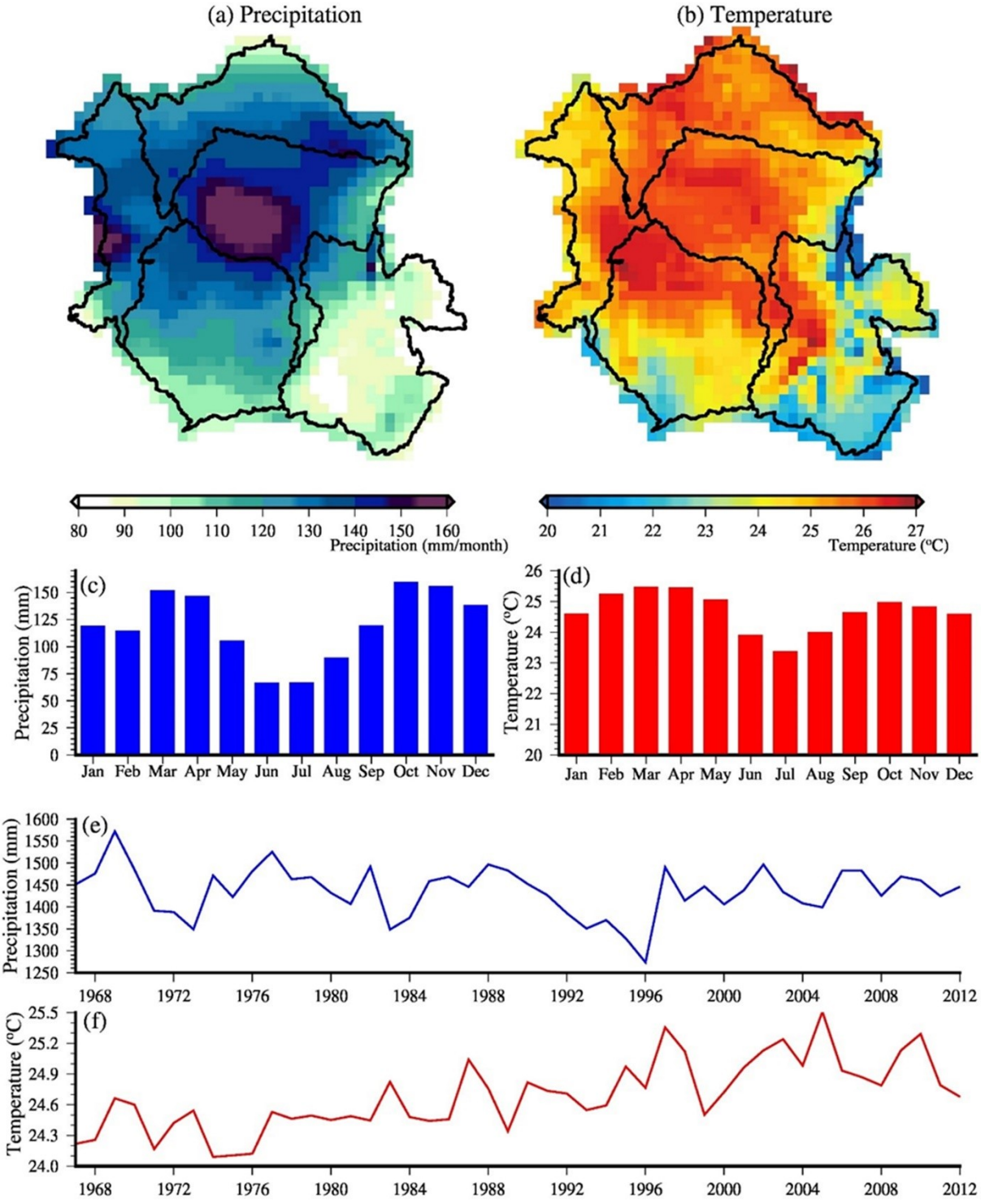
(a) Precipitation
(b) Temperature
80 90 100 110 120 130 140 150 160
Precipitation (mm/month)
20 21 22 23 24 25 26 27
Temperature (°C)
(c)
Precipitation (mm)
0 25 50 75 100 125 150
Jan Feb Mar Apr May Jun Jul Aug Sep Oct Nov Dec
(d)
Temperature (°C)
20 21 22 23 24 25 26
Jan Feb Mar Apr May Jun Jul Aug Sep Oct Nov Dec
(e)
Precipitation (mm)
1250 1300 1350 1400 1450 1500 1550 1600
1968 1972 1976 1980 1984 1988 1992 1996 2000 2004 2008 2012
(f)
Temperature (°C)
24.0 24.3 24.6 24.9 25.2 25.5
1968 1972 1976 1980 1984 1988 1992 1996 2000 2004 2008 2012

Figure 2.

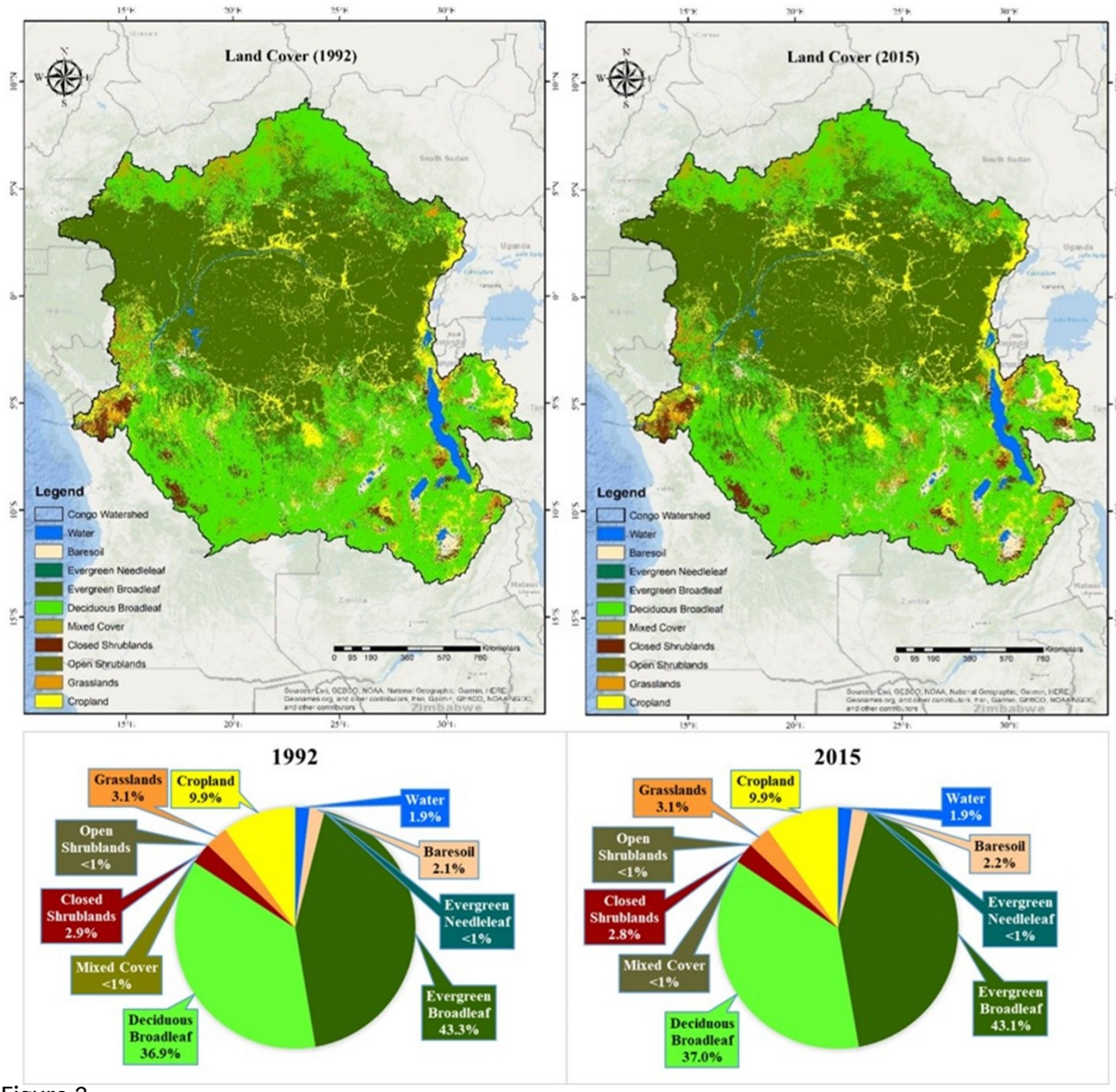
Land Cover (1992)
Land Cover (2015)
Legend
Congo Watershed
Water
Baresoil
Evergreen Needleleaf
Evergreen Broadleaf
Deciduous Broadleaf
Mixed Cover
Closed Shrublands
Open Shrublands
Grasslands
Cropland
1992
Grasslands 3.1%
Cropland 9.9%
Water 1.9%
Open Shrublands <1%
Baresoil 2.1%
Closed Shrublands 2.9%
Evergreen Needleleaf <1%
Mixed Cover <1%
Evergreen Broadleaf 43.3%
Deciduous Broadleaf 36.9%
2015
Grasslands 3.1%
Cropland 9.9%
Water 1.9%
Open Shrublands <1%
Baresoil 2.2%
Closed Shrublands 2.8%
Evergreen Needleleaf <1%
Mixed Cover <1%
Evergreen Broadleaf 43.1%
Deciduous Broadleaf 37.0%

Figure 3.

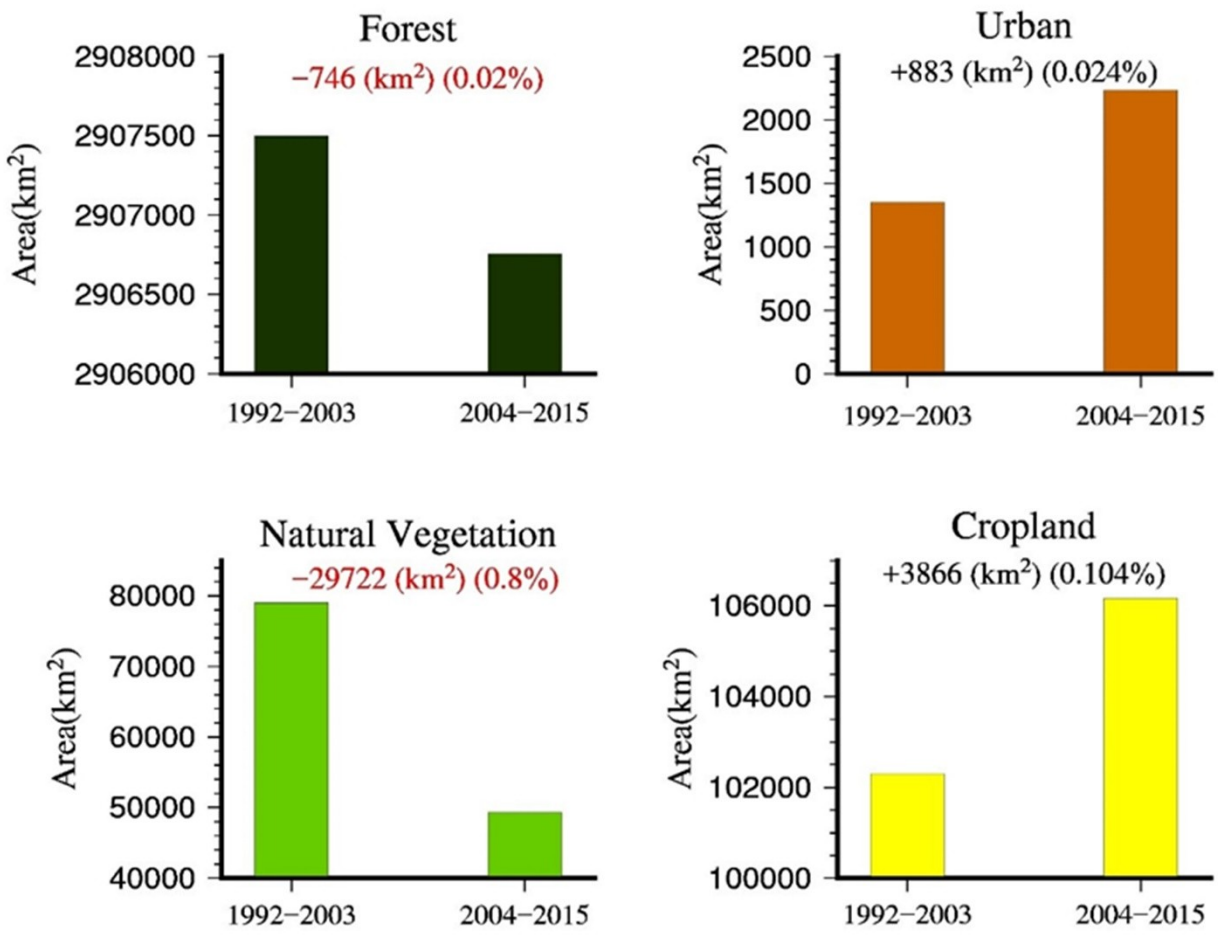

649
650 Figure 4.
651

73

74

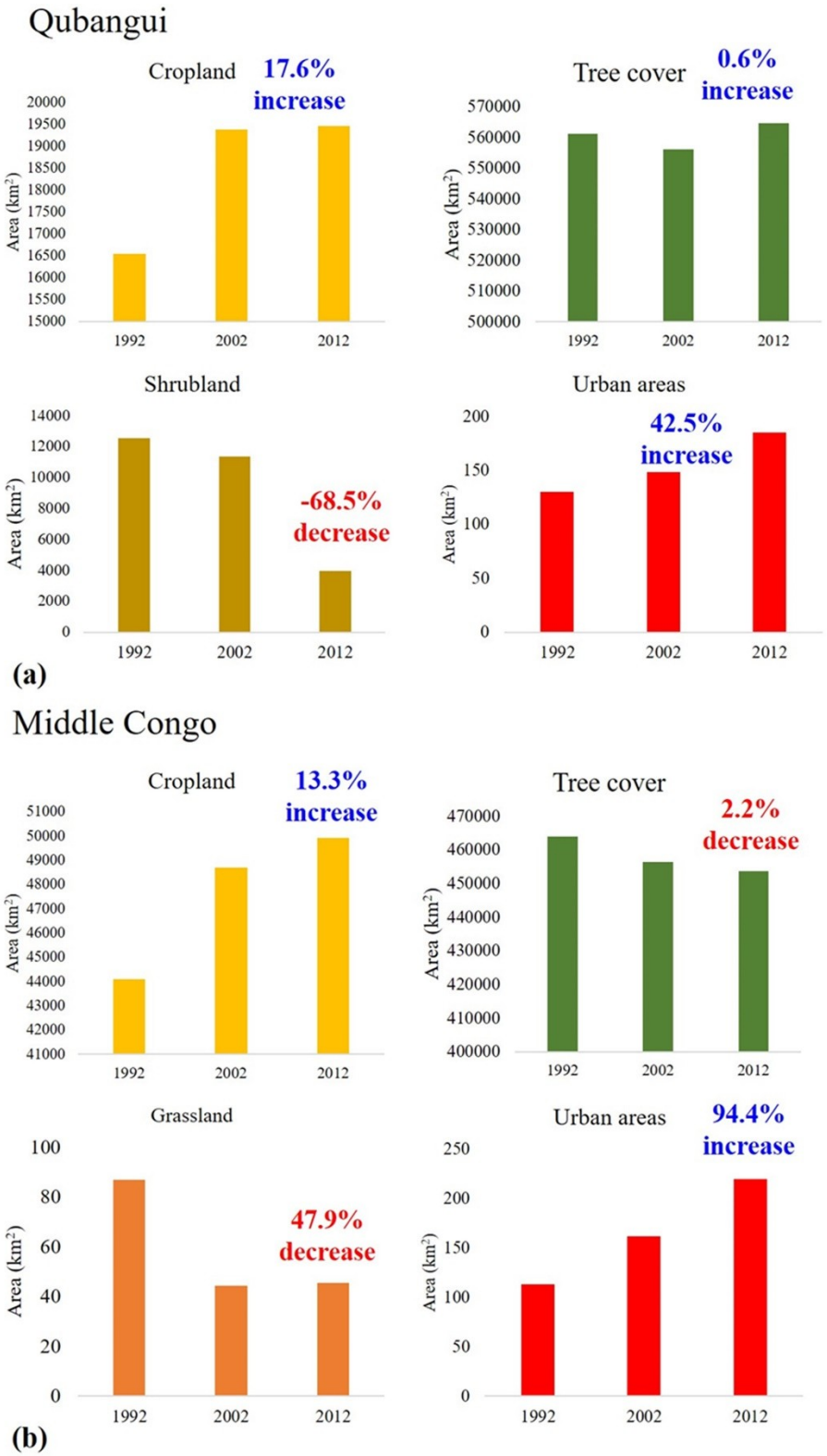
Qubangui
Cropland
17.6% increase
Tree cover
0.6% increase
Shrubland
-68.5% decrease
Urban areas
42.5% increase
Area (km²)
1992
2002
2012
(a)
Middle Congo
Cropland
13.3% increase
Tree cover
2.2% decrease
Grassland
47.9% decrease
Urban areas
94.4% increase
(b)

Figure 5.

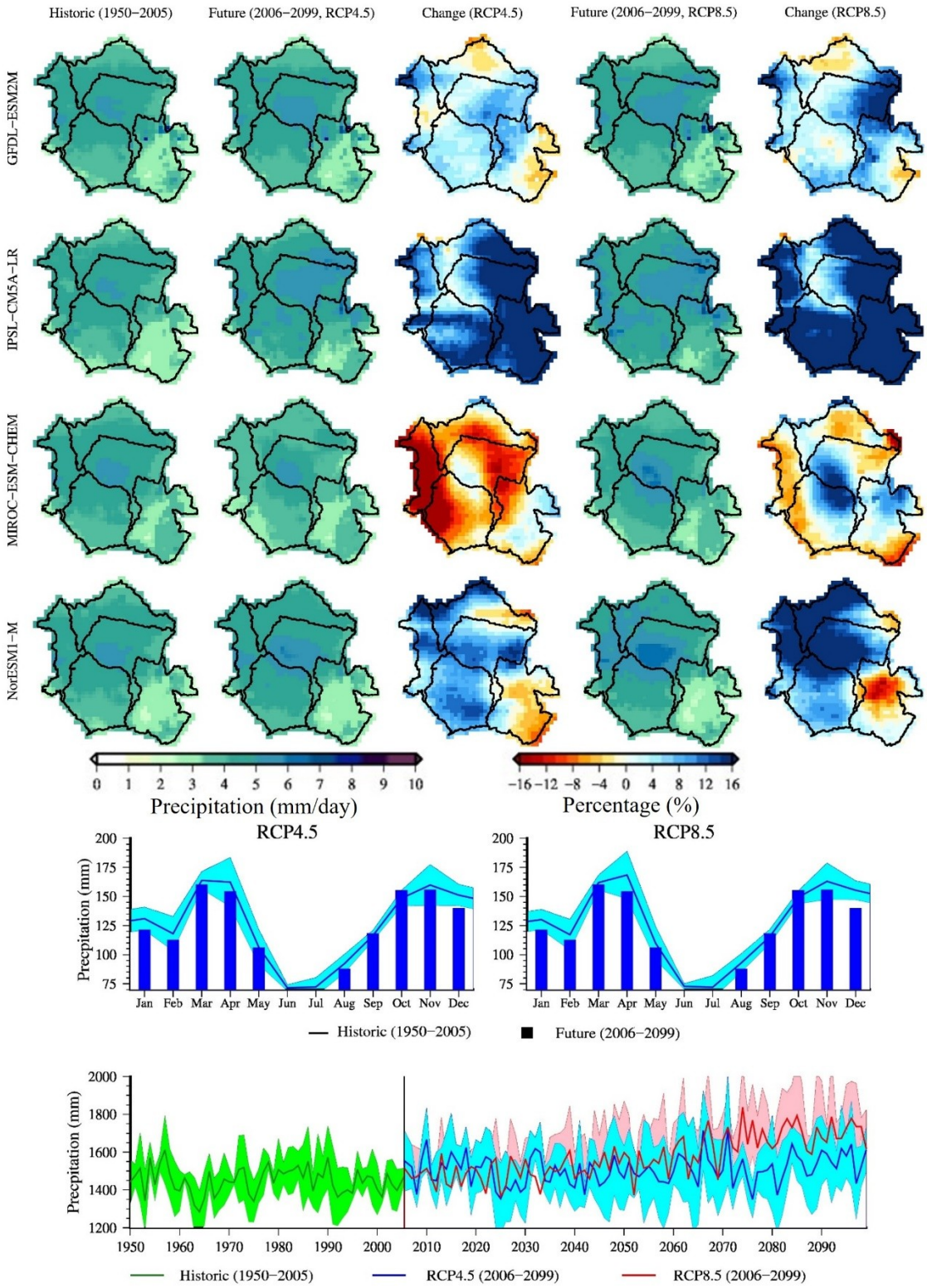
Historic (1950–2005)
Future (2006–2099, RCP4.5)
Change (RCP4.5)
Future (2006–2099, RCP8.5)
Change (RCP8.5)
GFDL–ESM2M
IPSL–CM5A–LR
MIROC–ESM–CHEM
NorESM1–M
0 1 2 3 4 5 6 7 8 9 10
Precipitation (mm/day)
−16 −12 −8 −4 0 4 8 12 16
Percentage (%)
RCP4.5
RCP8.5
Precipitation (mm)
Jan Feb Mar Apr May Jun Jul Aug Sep Oct Nov Dec
Historic (1950–2005)
Future (2006–2099)
Precipitation (mm)
1950 1960 1970 1980 1990 2000 2010 2020 2030 2040 2050 2060 2070 2080 2090
Historic (1950–2005)
RCP4.5 (2006–2099)
RCP8.5 (2006–2099)

Figure 6.

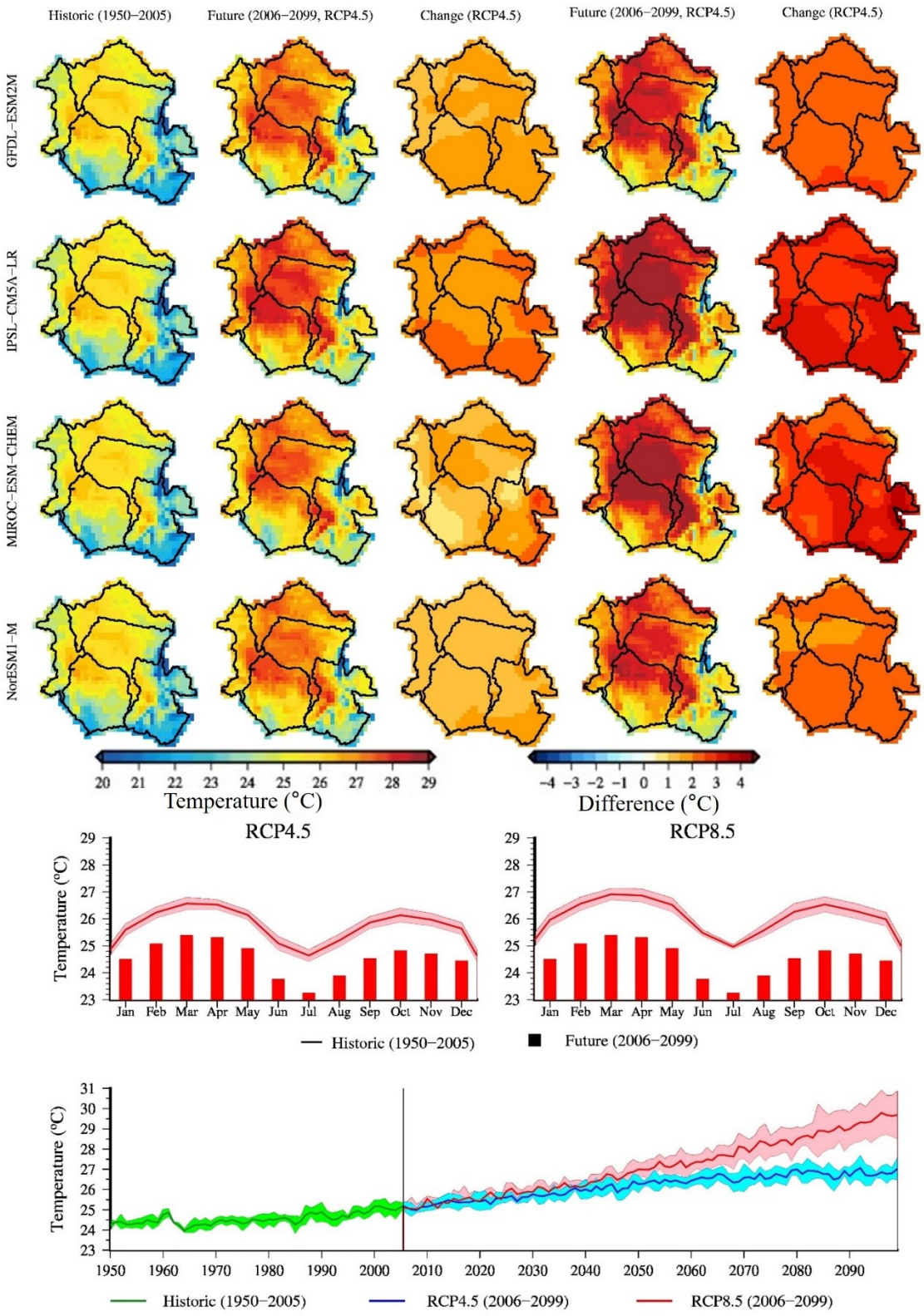
Historic (1950–2005)
Future (2006–2099, RCP4.5)
Change (RCP4.5)
Future (2006–2099, RCP4.5)
Change (RCP4.5)
GFDL–ESM2M
IPSL–CM5A–LR
MIROC–ESM–CHEM
NorESM1–M
20 21 22 23 24 25 26 27 28 29
Temperature (°C)
−4 −3 −2 −1 0 1 2 3 4
Difference (°C)
RCP4.5
RCP8.5
Temperature (°C)
Jan Feb Mar Apr May Jun Jul Aug Sep Oct Nov Dec
Historic (1950–2005)
Future (2006–2099)
1950 1960 1970 1980 1990 2000 2010 2020 2030 2040 2050 2060 2070 2080 2090
Historic (1950–2005)
RCP4.5 (2006–2099)
RCP8.5 (2006–2099)

Figure 7.

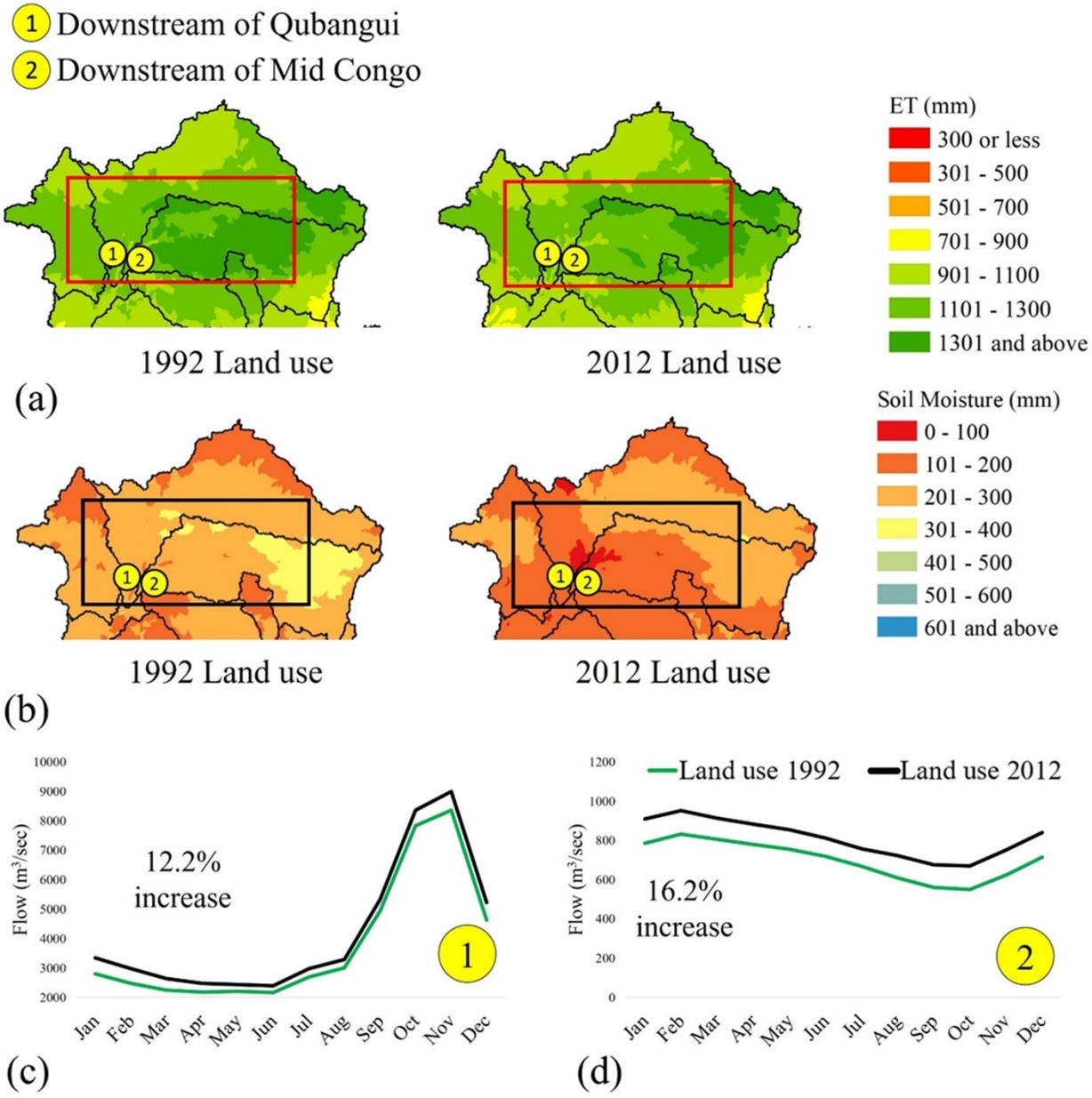
1 Downstream of Qubangui
2 Downstream of Mid Congo
ET (mm)
300 or less
301 - 500
501 - 700
701 - 900
901 - 1100
1101 - 1300
1301 and above
1992 Land use
2012 Land use
(a)
Soil Moisture (mm)
0 - 100
101 - 200
201 - 300
301 - 400
401 - 500
501 - 600
601 and above
1992 Land use
2012 Land use
(b)
Flow (m³/sec)
12.2% increase
1
Jan Feb Mar Apr May Jun Jul Aug Sep Oct Nov Dec
(c)
Land use 1992
Land use 2012
Flow (m³/sec)
16.2% increase
2
Jan Feb Mar Apr May Jun Jul Aug Sep Oct Nov Dec
(d)

Figure 8.

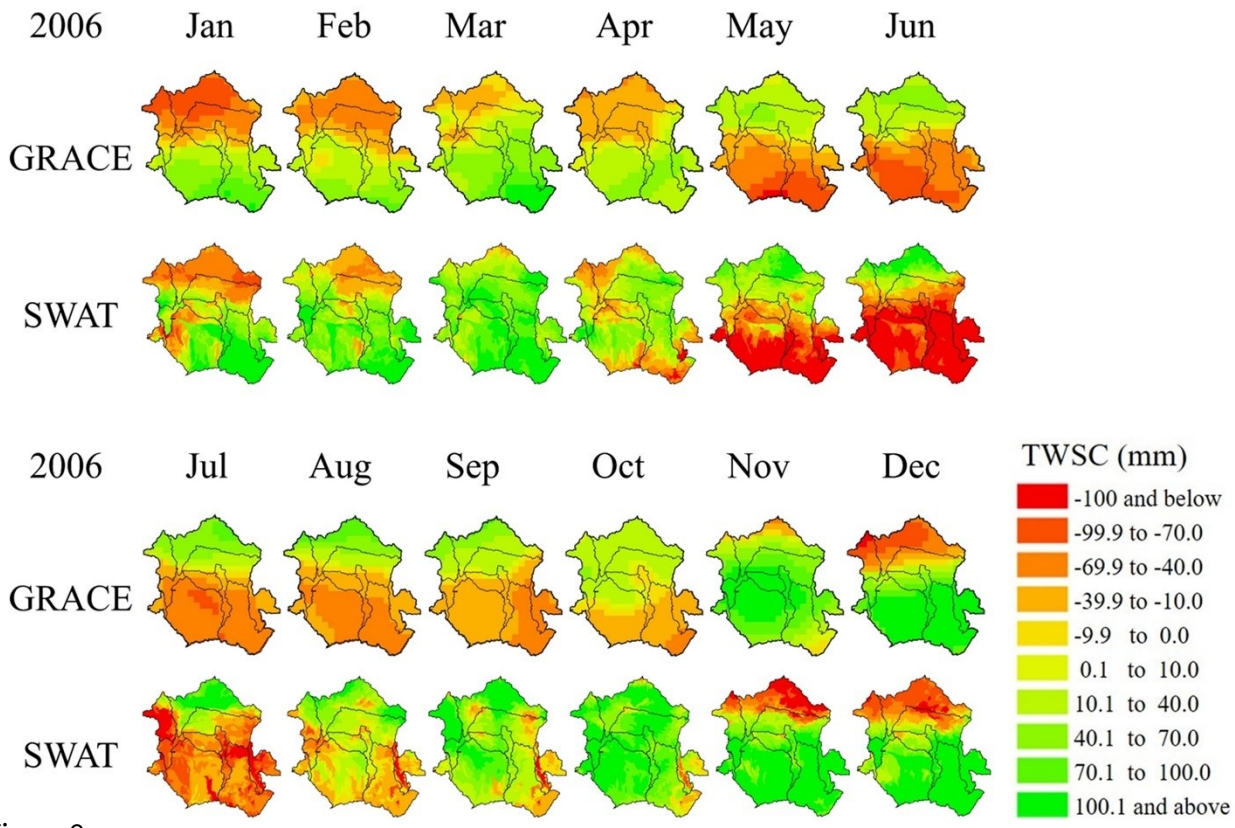
2006
Jan
Feb
Mar
Apr
May
Jun
GRACE
SWAT
2006
Jul
Aug
Sep
Oct
Nov
Dec
GRACE
SWAT
TWSC (mm)
-100 and below
-99.9 to -70.0
-69.9 to -40.0
-39.9 to -10.0
-9.9 to 0.0
0.1 to 10.0
10.1 to 40.0
40.1 to 70.0
70.1 to 100.0
100.1 and above

Figure 9.

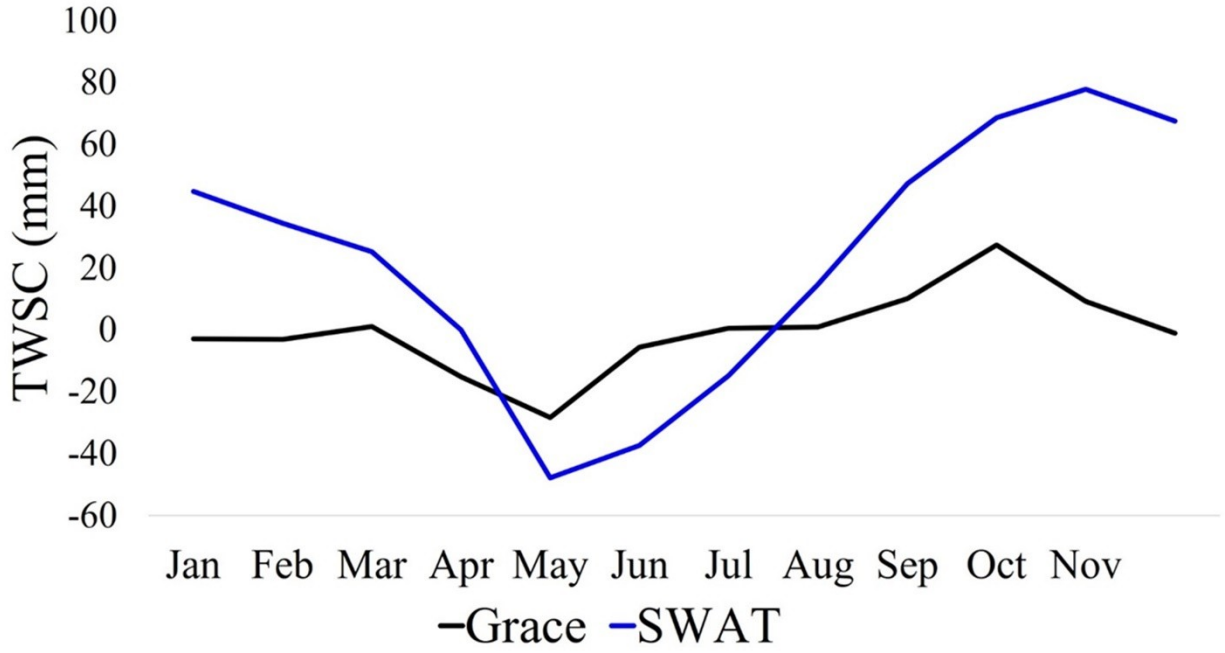
100
80
60
40
20
0
-20
-40
-60
TWSC (mm)
Jan
Feb
Mar
Apr
May
Jun
Jul
Aug
Sep
Oct
Nov
Grace
SWAT

Figure 10.

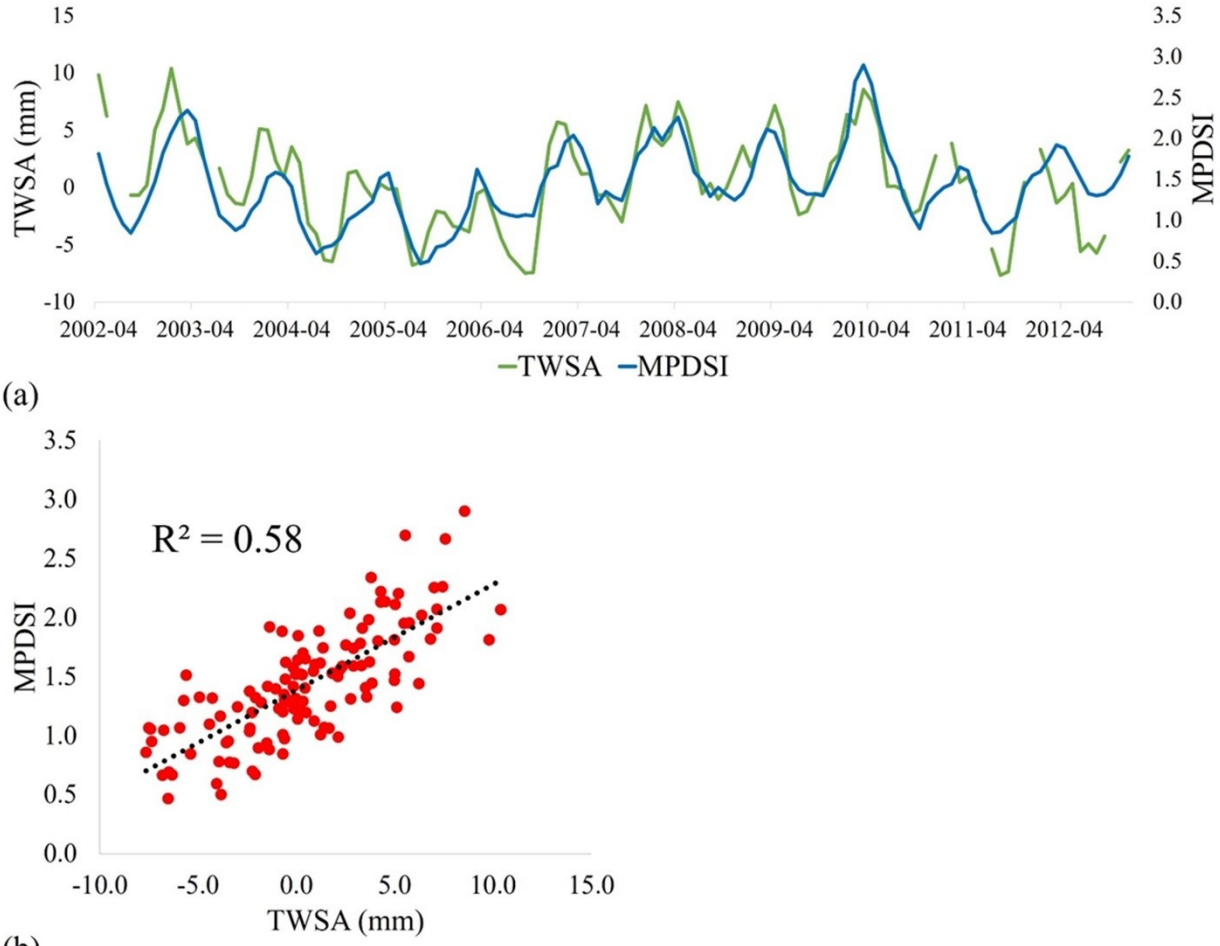
15
10
5
0
-5
-10
TWSA (mm)
3.5
3.0
2.5
2.0
1.5
1.0
0.5
0.0
MPDSI
2002-04
2003-04
2004-04
2005-04
2006-04
2007-04
2008-04
2009-04
2010-04
2011-04
2012-04
TWSA
MPDSI
(a)
R² = 0.58
MPDSI
TWSA (mm)
-10.0
-5.0
0.0
5.0
10.0
15.0
(b)

Figure 11.

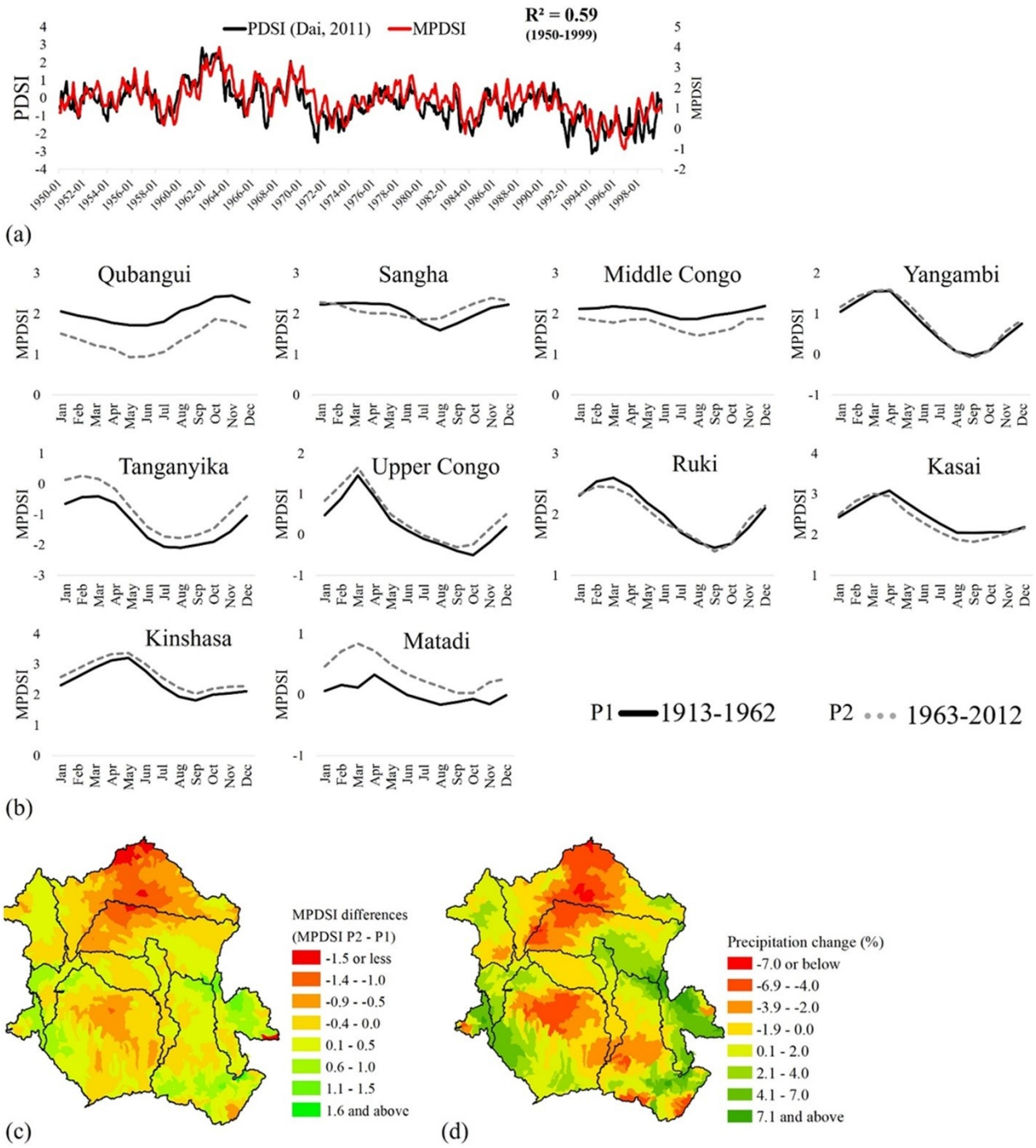
PDSI (Dai, 2011)
MPDSI
R² = 0.59
(1950-1999)
PDSI
MPDSI
(a)
Qubangui
Sangha
Middle Congo
Yangambi
Tanganyika
Upper Congo
Ruki
Kasai
Kinshasa
Matadi
MPDSI
Jan Feb Mar Apr May Jun Jul Aug Sep Oct Nov Dec
P1 1913-1962
P2 1963-2012
(b)
MPDSI differences
(MPDSI P2 - P1)
-1.5 or less
-1.4 - -1.0
-0.9 - -0.5
-0.4 - 0.0
0.1 - 0.5
0.6 - 1.0
1.1 - 1.5
1.6 and above
(c)
Precipitation change (%)
-7.0 or below
-6.9 - -4.0
-3.9 - -2.0
-1.9 - 0.0
0.1 - 2.0
2.1 - 4.0
4.1 - 7.0
7.1 and above
(d)

Figure 12.

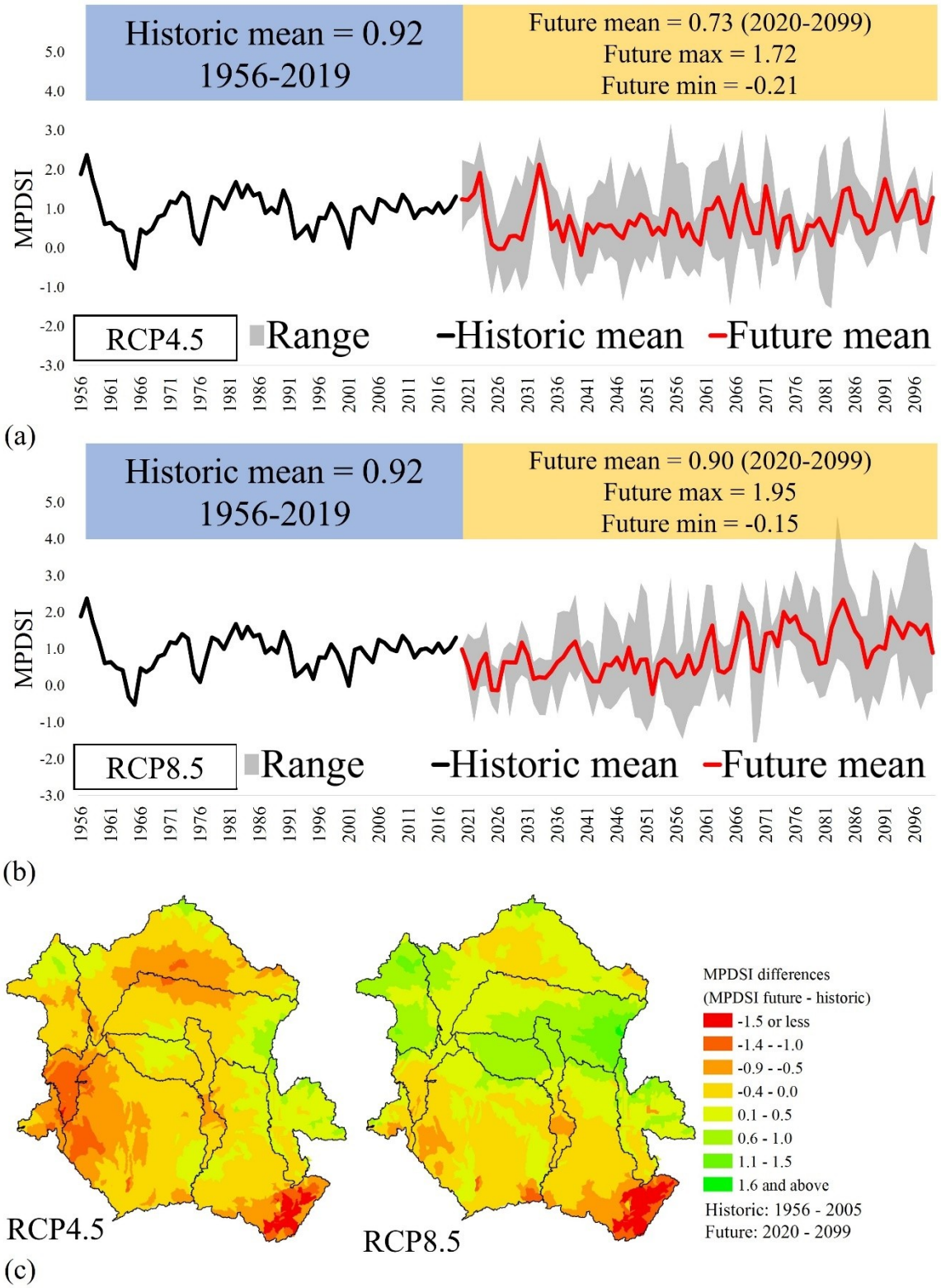
Historic mean = 0.92
1956-2019
Future mean = 0.73 (2020-2099)
Future max = 1.72
Future min = -0.21
MPDSI
RCP4.5
Range
Historic mean
Future mean
(a)
Historic mean = 0.92
1956-2019
Future mean = 0.90 (2020-2099)
Future max = 1.95
Future min = -0.15
MPDSI
RCP8.5
Range
Historic mean
Future mean
(b)
RCP4.5
RCP8.5
MPDSI differences
(MPDSI future - historic)
-1.5 or less
-1.4 - -1.0
-0.9 - -0.5
-0.4 - 0.0
0.1 - 0.5
0.6 - 1.0
1.1 - 1.5
1.6 and above
Historic: 1956 - 2005
Future: 2020 - 2099
(c)

Figure 13.

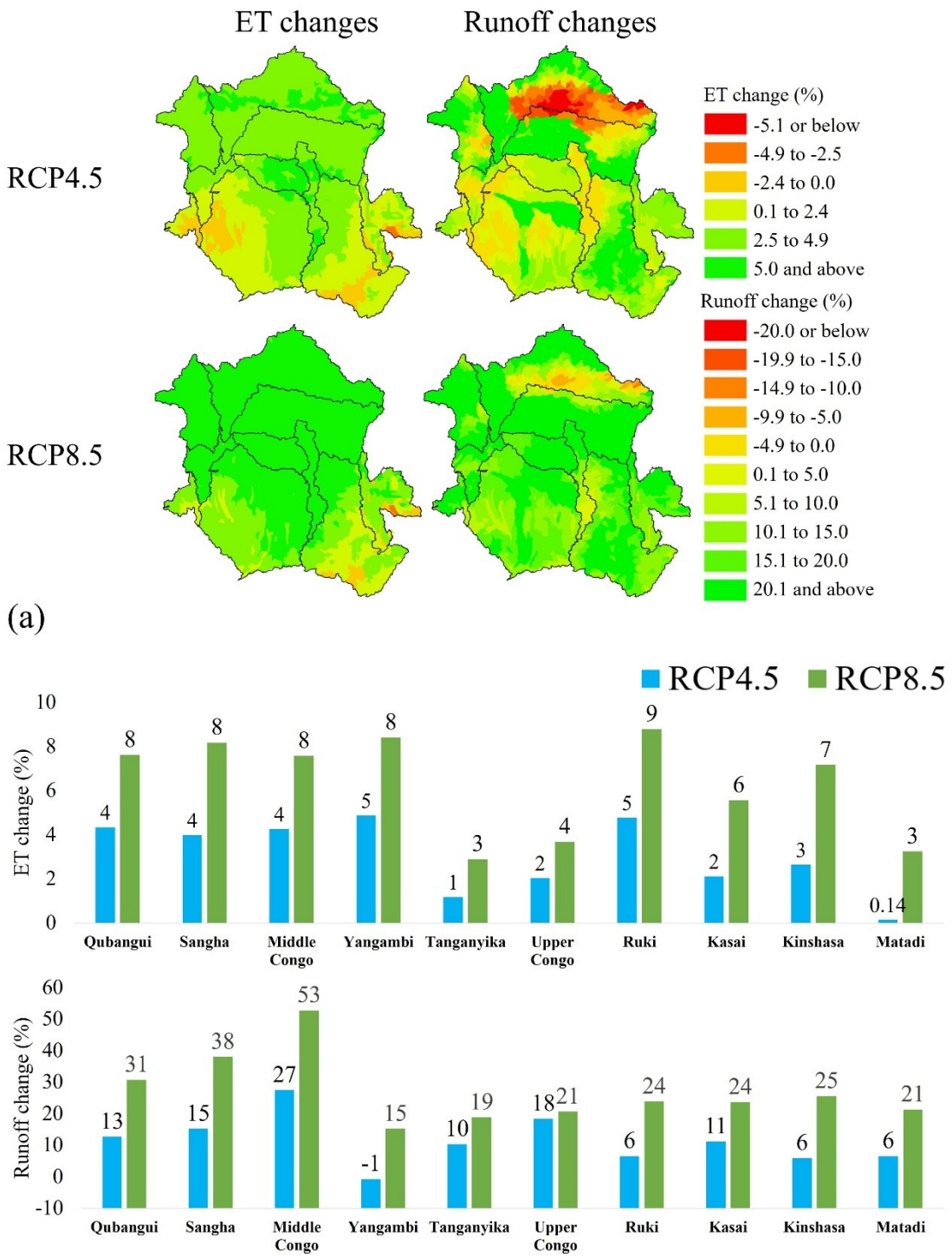

676

677
678 Figure 14.
679

93

94

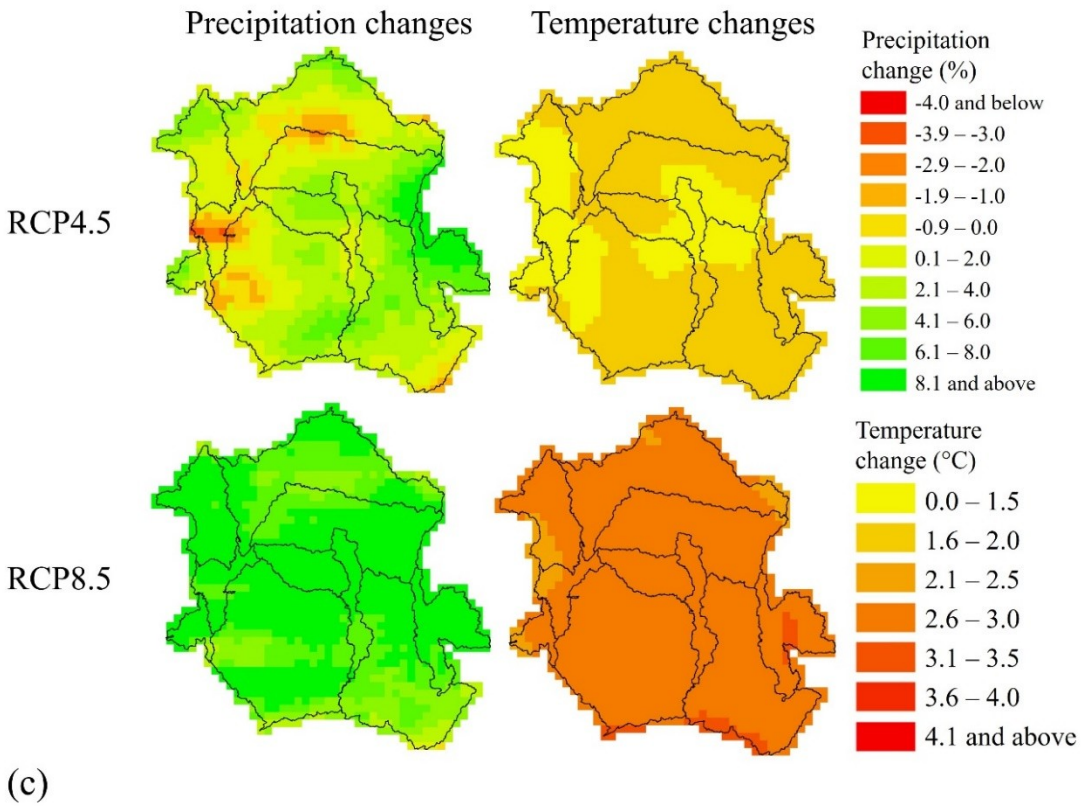

Figure 14 - continued.